

12

ADA 132455

Interim Report
6/16/82 - 6/15/83

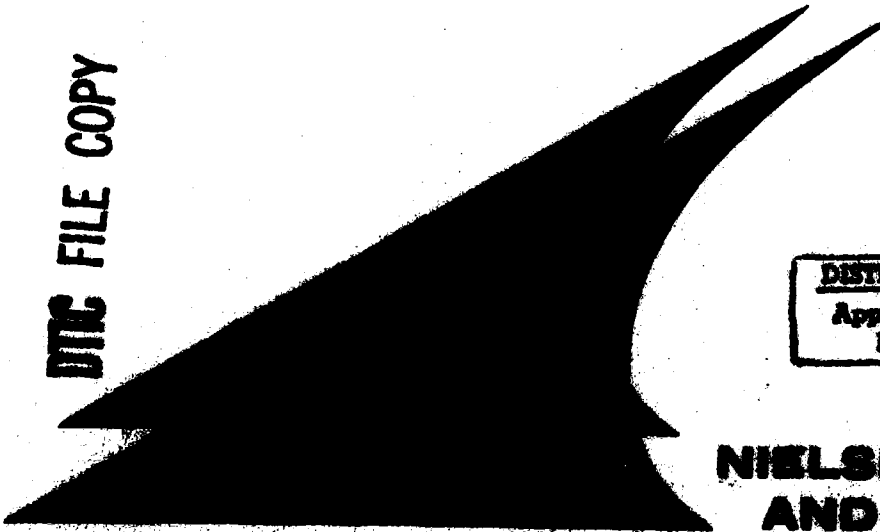
TRISERVICE PROGRAM FOR EXTENDING MISSILE
AERODYNAMIC DATA BASE AND PREDICTION
PROGRAM USING RATIONAL MODELING

by

Michael J. Hensch and Jack N. Nielsen

DTIC FILE COPY

DTIC
ELECTE
SEP 14 1983
S D
B



DISTRIBUTION STATEMENT A
Approved for public release,
Distribution Unlimited

**NIELSEN ENGINEERING
AND RESEARCH, INC.**

OFFICE: 510 CLYDE AVENUE / MOUNTAIN VIEW, CALIFORNIA 94043 / TELEPHONE (415) 960-6887

83 09 13 027

Interim Report
6/16/82 - 6/15/83

TRISERVICE PROGRAM FOR EXTENDING MISSILE
AERODYNAMIC DATA BASE AND PREDICTION
PROGRAM USING RATIONAL MODELING

by

Michael J. Hensch and Jack N. Nielsen

NEAR TR 305
August 1983

Prepared Under Contract No. N00014-80-C-0700

for

OFFICE OF NAVAL RESEARCH
Arlington, Virginia 22217

by

NIELSEN ENGINEERING & RESEARCH, INC.
510 Clyde Avenue, Mountain View, CA 94043
Telephone (415) 968-9457

DTIC
ELECTE
SEP 14 1983

B

DISTRIBUTION STATEMENT A
Approved for public release;
Distribution Unlimited

UNCLASSIFIED

SECURITY CLASSIFICATION OF THIS PAGE (When Data Entered)

REPORT DOCUMENTATION PAGE		READ INSTRUCTIONS BEFORE COMPLETING FORM
1. REPORT NUMBER	2. GOVT ACCESSION NO. AD-A132455	3. RECIPIENT'S CATALOG NUMBER
4. TITLE (and Subtitle) TRISERVICE PROGRAM FOR EXTENDING MISSILE AERODYNAMIC DATA BASE AND PREDICTION PRO- GRAM USING RATIONAL MODELING		5. TYPE OF REPORT & PERIOD COVERED Interim Report 40.3 6/16/82 - 6/15/83
7. AUTHOR(s) Michael J. Hensch Jack N. Nielsen		6. PERFORMING ORG. REPORT NUMBER NEAR TR 305
9. PERFORMING ORGANIZATION NAME AND ADDRESS Nielsen Engineering & Research, Inc. 510 Clyde Avenue Mountain View, CA 94043		8. CONTRACT OR GRANT NUMBER(s) N00014-80-C-0700
11. CONTROLLING OFFICE NAME AND ADDRESS Office of Naval Research 800 North Quincy Street Arlington, Virginia 22217		10. PROGRAM ELEMENT, PROJECT, TASK AREA & WORK UNIT NUMBERS
14. MONITORING AGENCY NAME & ADDRESS (if different from Controlling Office)		12. REPORT DATE August 1983
		13. NUMBER OF PAGES 78
		15. SECURITY CLASS. (of this report) UNCLASSIFIED
		15a. DECLASSIFICATION/DOWNGRADING SCHEDULE
16. DISTRIBUTION STATEMENT (of this Report) Approved for public release; distribution unlimited		
17. DISTRIBUTION STATEMENT (of the abstract entered in Block 20, if different from Report)		
18. SUPPLEMENTARY NOTES		
19. KEY WORDS (Continue on reverse side if necessary and identify by block number) Missile Aerodynamics Wind Tunnel Tests Computer Programs		
20. ABSTRACT (Continue on reverse side if necessary and identify by block number) The work described in this report was accomplished during the third year of the Triservice program for extending the missile aerodynamic data base and incorporating the new data into the predictive program known as MISSILE. The work consisted of four aspects: (1) support of the ongoing wind tunnel tests, (2) preparation for processing the data to be incorporated into the data base, (3) methods development, and (4) code development.		

DD FORM 1 JAN 73 1473 EDITION OF 1 NOV 65 IS OBSOLETE

UNCLASSIFIED
SECURITY CLASSIFICATION OF THIS PAGE (When Data Entered)

TABLE OF CONTENTS

<u>Section</u>	<u>Page No.</u>
1. INTRODUCTION	3
2. REVIEW OF THE DATA	6
2.1 Control-Effectiveness for Transonic Flow	6
2.2 Control-Effectiveness for Supersonic Flow	6
3. ANALYSIS OF THE CONTROL-EFFECTIVENESS DATA FOR SUPERSONIC FLOW	8
3.1 Correlation of the Data	8
3.2 Implications for the Equivalent Angle-of-attack Concept and MISSILE 3	10
4. DATA PROCESSING	12
5. ANALYSIS OF PROPOSED BODY ALONE NORMAL-FORCE AND PITCHING-MOMENT METHODOLOGY	13
5.1 Candidate Formulations - Normal Force Coefficient	13
5.2 Candidate Formulations - Center of Pressure	15
5.3 Data Base for $C_{N\alpha}$ and x_{cp0}	16
5.4 Comparisons with Data	17
5.5 Conclusions	19
6. CONCLUDING REMARKS	20
REFERENCES	21
TABLE 1	23
FIGURES 1 THROUGH 29	24
NOMENCLATURE	77

1. INTRODUCTION

Under Office of Naval Research Contract No. N00014-80-C-0700, Nielsen Engineering & Research, Inc. (NEAR) has been funded to obtain the necessary fin data base for broadly applicable engineering prediction programs for calculating the aerodynamic characteristics of body-tail and canard (wing)-body-tail missiles. Under the same contract, the data base will be incorporated into one specific computer program called PROGRAM MISSILE (refs. 1 and 2) which is valid for angles of attack up to 45° and arbitrary roll angle. The first year's work involved: (1) selection of the test model design, test parameters and testing sequence, (2) preliminary investigation of the optimum approach for data handling, i.e., preparing the data for and incorporating it into PROGRAM MISSILE and (3) revising the equivalent angle-of-attack formulation to incorporate the new fin deflection data base. The results of that work are described in the first year's report (ref. 3). The second year's work consisted of (1) support of the ongoing wind tunnel tests, (2) preparation for processing the data to be incorporated into the data base, (3) continued improvement of the methods used in MISSILE and (4) continued code development. The results of that work are described in the second year's report (ref. 4). The third year's work continued the activities of the second year.

Six tunnel entries have been planned. The three high Mach number (2.5 - 4.5) tests were to be conducted in the NASA/Langley Unitary Plan Tunnel, Section 2. The first and second Langley entries were completed in May 1982 and July 1983 respectively. The three low and intermediate Mach number (0.6 - 2.0) tests will be conducted in the 6- by 6-foot Supersonic Tunnel at NASA/Ames. The first Ames entry was completed in January 1983. The second Ames entry is now scheduled for January 1984.

At the writing of this report, all of the $\delta = 0$ data for the control fins have been obtained. Because of problems with

the low-aspect-ratio fin balances, no data for those fins has been obtained. The low-AR fins will be tested in the third entry at NASA/Langley and in the second entry at NASA/Ames. The status of the control ($\delta \neq 0$) data is given in the table below. An "X" means that the data have been obtained.

Required Control Fin Data Base ($\delta \neq 0$)

FIN	M_∞ Angle-of-attack range	NASA/ARC			NASA/LRC	
		0.8	1.2	2.0	3.0	4.5
42 AR=1 $\lambda=1/2$	low				X	X
	high					
51 AR=2 $\lambda=0$	low	X	X	X	X	X
	high				X	X
52 AR=2 $\lambda=1/2$	low	X	X	X	X	X
	high				X	X
53 AR=2 $\lambda=1$	low		X		X	X
	high				X	X
62 AR=4 $\lambda=2$	low					
	high					

The next section presents some representative data from the first entries at NASA/ARC and NASA/LRC. In the third section an analysis is presented of some of the high Mach number control effectiveness data. The analysis leads to some important conclusions regarding the rational modeling to be used in the data-base prediction program (MISSILE 3). In section 4 a discussion of some of the data processing methodology is presented including changes which are required as a result of the findings of section 3. In section 5 an extensive analysis of the proposed body alone methodology is presented. Concluding remarks are given in section 6.

2. REVIEW OF THE DATA

2.1 Control-Effectiveness for Transonic Flow

Some sample transonic results from the first entry at NASA/ARC are given in figure 1. The sign conventions are given in figure 2. The data are for the aspect ratio 2 control fins at $\alpha_c = 20^\circ$ with taper ratios equal to 0, 1/2 and 1. Only the normal-force coefficient for the one deflected fin is shown. Important things to note are (1) the change in taper ratio effects with Mach number and (2) the significantly smaller control effectiveness for $\delta = 40^\circ$ compared to $\delta = -40^\circ$.

2.2 Control-Effectiveness for Supersonic Flow

Typical normal-force coefficient data from both of the entries are presented as a function of bank angle in figure 3 for the deflected fin for a body incidence angle of 20° . The reference area is the fin planform area. There are two features which should be noted. First, the shape of the $\delta_2 = 0$ curves is familiar from previous work (e.g., ref. 5). The maximum value of the normal-force coefficient is displaced toward the windward side from the horizontal symmetry position of $\phi = 0$ to roughly $\phi = 25^\circ$ in accordance with slender-body theory, and the peak values of $C_{NF(B)}$ decrease with M_∞ as would be expected. Note also that the negative values of $C_{NF(B)}$ for the $\delta_2 = 0$ cases are much smaller for $M_\infty = 3.0$ and 4.5 indicating a change in vortical flow properties.

The second feature of note is the changing control effectiveness with increasing Mach number. In particular, compare the normal-force coefficients at $\phi = -90^\circ$ (leeward plane) and $\phi = +90^\circ$ (windward plane). For $\delta_2 = 0$, $C_{NF(B)}$ at $\phi = \pm 90^\circ$ is zero; hence, the values shown for $\delta_2 \neq 0$ represent control effectiveness only. For $M_\infty = 2.00$, the control effectiveness for $\phi = 90^\circ$ is slightly greater than for $\phi = -90^\circ$. As M_∞ is increased the control effectiveness at $\phi = -90^\circ$ decreases

sharply to negligible values while the effectiveness at $\phi = 90^\circ$ increases. Note also that, for certain values of ϕ on the windward side, $C_{NF(B)}$ is greater than the maximum value of 1.7 given by Hoerner (ref. 6) for a flat plate normal to the free stream! An additional set of data for the same fin but with $\alpha_c = 35^\circ$ and $M_\infty = 3.0$ is given in figure 4. Note the similarity of the curves of figure 4 with those of figure 3(c) which have roughly the same cross flow Mach number.

An interesting perspective on the phenomenon described above can be gained by plotting the fin normal-force coefficient for the $\phi = \pm 90^\circ$ positions as a function of cross flow Mach number, $M_c = M_\infty \sin \alpha_c$. This is done for $M_\infty = 2.0, 3.0$ and 4.5 and fin deflection angles of $\pm 20^\circ$ in figure 5. The fin normal-force coefficient for a given α_c is normalized by its value at $\alpha_c = 0$ to give the curves a common value at $M_c = 0$. Figure 5 shows that the data correlate fairly well with cross flow Mach number.

It is obvious from figure 5 that a yaw command in the plus configuration for a high cross flow Mach number will lead to an induced rolling moment which will have to be answered by the horizontal fins. However, when a high performance missile is pulling a high-g maneuver, much of the available horizontal fin deflection capability will be used to trim the vehicle in the pitch plane. Hence, little will be left to counter any induced rolling moment due to a yaw command. Clearly, this would put a limit on the α_c which the vehicle could safely reach for high cross flow Mach numbers.

3. ANALYSIS OF THE CONTROL-EFFECTIVENESS DATA FOR SUPERSONIC FLOW

3.1 Correlation of the Data

The large variation in $C_{NF(B)}$ with fin bank angle and the correlation of figure 5 prompts us to consider the local flow field property variation around the body alone. To do this we used the SWINT marching Euler solver (ref. 7) which has the capability of shedding and convecting vorticity at prescribed separation lines on the body. The separation line locations were determined from a correlation by Nielsen (ref. 8) made from Landrum's oil-flow data (ref. 9). A series of runs were made on a 3-caliber cone-cylinder for various Mach numbers and angles of attack. After the runs were made a postprocessor was used to compute the local dynamic pressure, q_ℓ , and Mach number, M_ℓ .

For the purposes of the present work, we will use values of q_ℓ and M_ℓ which have been averaged over the exposed span of the fin,* i.e.

$$\bar{q}_\ell \equiv \frac{1}{s_m - a} \int_a^{s_m} q_\ell(\phi, r) dr \quad (1)$$

$$\bar{M}_\ell \equiv \frac{1}{s_m - a} \int_a^{s_m} M_\ell(\phi, r) dr \quad (2)$$

Hence, for the data presented here the integration interval was from a to $2a$. The computed results for \bar{q}_ℓ and \bar{M}_ℓ at 10 diameters aft of the nose tip for a body incidence angle of 20° are given in figure 6.

It is immediately apparent from the results shown in figure 6 that the variations of both the local Mach number and dynamic

*The averaging was applied along the radial line defined by the exposed fin span for $\delta = 0$ as if the fin were immersed in the body alone flow field.

pressure contribute to the behavior displayed in figures 3 - 5. At $M_\infty = 1.60$, for example, both \bar{q}_ℓ and \bar{M}_ℓ vary only slightly with ϕ from their free stream values. However, as M_∞ increases, the variation with ϕ of both quantities increases. At $M_\infty = 4.63$ and $\phi = 90^\circ$, for instance, $\bar{q}_\ell/q_\infty = 2.07$ and $\bar{M}_\ell = 3.5$. Both of these flow field values would contribute to higher-than-expected values of $C_{NF(B)}$ when the fin is deflected, the lower Mach number giving a higher wing-alone, normal-force coefficient slope.

Given the above results, it seems reasonable to conjecture that the wide variation in $C_{NF(B)}$ seen in figures 3 - 5 is due to local flow field property variations caused by the presence of the body alone. This conjecture can be checked by using the equivalent angle-of-attack concept of Appendix A of the first year's report (ref. 3) and the local flow field property values of figure 6. Since only fin 2 of the model was deflected we can write equation (A-10) of reference 3 as

$$\alpha_{eq_2} = \hat{\alpha}_{eq_2} + \Lambda_{22}\delta_2 \quad (3)$$

or

$$\Lambda_{22} = (\alpha_{eq_2} - \hat{\alpha}_{eq_2})/\delta_2 \quad (4)$$

If the conjecture is correct, it should be possible to use equation (4) to collapse the δ and ϕ dependence of the data in figures 3 and 4.

The steps which were used to check the conjecture for a given body angle of attack and free stream Mach number are as follows:

1. For particular values of ϕ , M_∞ and α_C , determine $C_{NF(B)}$ from the data for $\delta_2 = 0, +20^\circ, +40^\circ$.
2. Multiply the results of step 1 by q_∞/\bar{q}_ℓ for the same values of ϕ , M_∞ and α_C to obtain $\bar{C}_{NF(B)}$ referenced to the (computed) local dynamic pressure.
3. Interpolate in the wing-alone data of reference 10 for wings with the same planform at the (computed) local Mach number to obtain values of α_{eq}

corresponding to the results of step 2. Ignore those data points which would require extrapolation of the wing-alone curves beyond $\alpha = 60^\circ$. The wing-alone curves (ref. 10) are given in figure 7.

4. Apply equation (2) to the results of step 3.

The results for the procedure above applied to the data of figures 3 and 4 are given in figures 8 and 9. It is clear that the correlation succeeds in taking out the ϕ dependence of the control effectiveness very well except for the bank angle region approximately $\pm 35^\circ$ from the leeward plane. The discrepancy near the leeward plane increases with M_∞ from hardly noticeable at $M_\infty = 2.0$ to more than a factor of 2 at $M_\infty = 4.5$. Hence, it seems safe to conclude that the Euler solver of reference 7 as implemented for the solution of figure 6 gives incorrect local flow field properties near the leeward plane for cross flow Mach numbers greater than one. However, because the loads under those conditions are relatively small for the a/s_m ratio tested (0.5), the error would not be particularly important. For smaller values of a/s_m , the error may be more important.

3.2 Implications for the Equivalent Angle-of-attack Concept and MISSILE 3

From the discussion in the subsection above, it is clear that the α_{eq} concept as outlined in Appendix A of reference 3 and in reference 5 will not accurately predict control effectiveness for cross flow Mach numbers greater than 0.5 because it is implied in the concept that \bar{q}_ℓ and \bar{M}_ℓ do not deviate from the free-stream conditions. However, with a reasonable amount of effort, the method can be extended so that it can still be used in the MISSILE 3 code to be developed under the present contract. To extend the α_{eq} concept to cross flow Mach numbers greater than 0.5 a table of \bar{q}_ℓ/q_∞ and \bar{M}_ℓ as functions of M_∞ , α_c , ϕ , a/s_m and x/D must be provided. For conditions under which the velocity parallel to the body axis is supersonic everywhere, such a table can be obtained relatively inexpensively using a marching Euler code with body vortex separation (e.g., ref. 7).

The region in which a marching code can be used is given in figure 10. As part of the work for the present effort, an extensive series of SWINT (ref. 7) runs were made to give the necessary body vortex properties for a body alone. These same runs will be used to make the needed MISSILE 3 table for \bar{q}_ℓ/q_∞ and \bar{M}_ℓ . For the region bounded by $M_c = 0.5$ and the shock-detachment boundary, an unsteady Navier-Stokes code will be needed. For the $M_c < 0.5$ region simple point-vortex "cloud" theory will be used to obtain the body vortex properties needed for MISSILE 3 since \bar{q}_ℓ and \bar{M}_ℓ do not vary significantly from the free stream values.

The actual steps required to extrapolate from the fin-on-body data base of MISSILE to different values of a/s_m , x/D and/or $(\Delta\alpha)_v$ are as follows:

1. For the M_∞ , α_c , ϕ , δ combination of interest, determine $C_{NF(B)}$ from data base.
2. Determine \bar{q}_ℓ/q_∞ and \bar{M}_ℓ for the ϕ location of interest for the a/s_m and x/D of the fin in the data base.
3. Divide the $C_{NF(B)}$ of step 1 by the \bar{q}_ℓ/q_∞ from step 2 to normalize it properly for use in the α_{eq} method.
4. For the wing-alone curve corresponding to the \bar{M}_ℓ of step 2, obtain α_{eq} for the normal-force coefficient resulting from step 3.
5. Using equations A(9) and A(10) of reference 3, determine the new α_{eq} for the conditions of interest.
6. Determine \bar{q}_ℓ/q_∞ and \bar{M}_ℓ for the ϕ location of interest for the a/s_m and x/D of interest.
7. For the α_{eq} of step 5 determine the C_{NW} corresponding to the \bar{M}_ℓ of step 6.
8. Multiply the C_{NW} of step 7 by the \bar{q}_ℓ/q_∞ of step 6 to get the $C_{NF(B)}$ of interest referenced to free stream conditions.

The steps above are illustrated in figure 11.

4. DATA PROCESSING

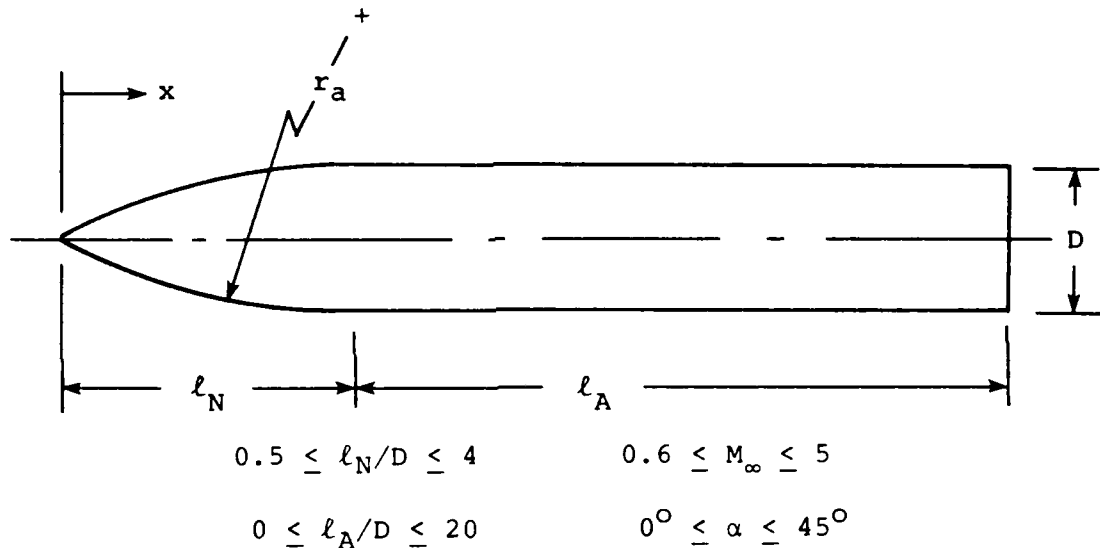
The portion of the data processing program which handles $\delta = 0$ cases without vortex asymmetry has been checked out using the data for fin 42 from the first entry at NASA/LRC. An example of the tabular output for fin normal-force coefficient is given in table 1. Results from the graphics routine which is used to check the normal-force coefficient tables (see subsection 3.4 of reference 4) are given in figure 12. Note the more "peaky" distribution for the higher Mach numbers.

Another task of the data processing program is the correlation of fin center-of-pressure location with fin normal-force coefficient. The algorithm used is a piecewise linear curve fit to the windward fin data (to minimize vortex effects) with smoothing based on minimization of the second derivatives. Typical results are given in figure 13. Note that the standard deviation is also given. It can be used in the new version of MISSILE to estimate the hinge- and bending-moment errors due to spread in the correlation. It was found that the amount of smoothing did not significantly change the standard deviations of the correlations. The quantity "GAMMA" is the relative amount of smoothing used.

For the correlations of figure 13, it was assumed that the measured normal-force coefficients are the appropriate values to use and that the Mach number seen by the fins is essentially M_∞ . In the previous section it is demonstrated that the above assumptions do not hold for high cross-flow Mach numbers. Consequently, it is expected that the correlation procedure used above will have to be altered so that nonlinear flow field effects can be taken into account. Preliminary work indicates that the correlations will change significantly and that the standard deviations of the correlations will be reduced.

5. ANALYSIS OF PROPOSED BODY ALONE NORMAL-FORCE AND PITCHING-MOMENT METHODOLOGY

In the following we extensively check two different formulations of the simplest crossflow drag method for predicting the normal force and location of the center-of-pressure for commonly encountered missile bodies alone using empirical input for $C_{N\alpha}$ and the center-of-pressure location for small α . The ranges of the parameters for pointed tangent-ogive noses in combination with right-circular-cylindrical bodies for which the formulations were checked are as follows:



5.1 Candidate Formulations - Normal Force Coefficient

The common starting point for the formulations considered is*

$$C_N = \frac{N}{q_\infty A_{ref}} = \sin 2\alpha + \eta c_{dc} \frac{A_p}{A_{ref}} \sin^2 \alpha \quad (5)$$

*The possible advantage of using an axial variation of the cross flow drag coefficient has not been considered in the present study.

where N is the resultant normal force on the body, c_{d_c} is the steady-state crossflow drag coefficient for an infinite circular cylinder, η is a correction factor for finite cylinder length, and A_p is the planform area of the body. The reference area used is the cross sectional area of the cylindrical portion of the body. This relation is a straightforward combination of slender-body theory ($\sin 2\alpha$) and a term representing the integrated force on the configuration due to viscous crossflow separation. In practice, the slender-body term has often been modified by the factor $\cos(\alpha/2)$, following Ward (ref. 11). With this modification, the above relation is that used in Reference 12. Note that at $\alpha = 90^\circ$,

$$C_N = \eta c_{d_c} A_p / A_{ref} \quad (6)$$

In the present work, one of our candidate formulations (Method A) is obtained from equation (5) as

$$C_N = \frac{C_{N_\alpha}}{2} \sin 2\alpha \cos \frac{\alpha}{2} + c_{d_c} \frac{A_p}{A_{ref}} \sin^2 \alpha \quad (7)$$

Inclusion of the additional factor $C_{N_\alpha}/2$ in the slender-body term allows for empirical input of the slope of the normal-force curve at $\alpha = 0^\circ$, instead of relying on the slender-body value ($C_{N_\alpha} = 2$). Additionally, we have set $\eta = 1$ to be used in conjunction with the modified curve for c_{d_c} discussed below.

The second candidate formulation is derived from Equation (5) as follows. The slender-body contribution to C_N is important only at small α , for which

$$\frac{C_{N_\alpha}}{2} \sin 2\alpha \cos \frac{\alpha}{2} \approx C_{N_\alpha} \sin \alpha \quad (8)$$

To maintain the result of equation (5) while using the approximation of equation (8), we must write

$$C_N = C_{N_\alpha} \sin \alpha + \left[c_{d_c} \frac{A_P}{A_{ref}} - C_{N_\alpha} \right] \sin^2 \alpha \quad (9)$$

Equation (9) will be called Method B.

5.2 Candidate Formulations - Center of Pressure

Both of the methods to be presented for calculating the location of the center of pressure (x_{cp}) are based on the assumption that the contribution to C_N from the C_{N_α} term (C_{NSB} , the term linear in $\sin \alpha$) acts for all α at the center-of-pressure location of the configuration at zero angle of attack (x_{cp0}), and the contribution from the cross-flow drag (C_{NV} , the term involving $\sin^2 \alpha$) acts at the centroid of the planform area (x_c). Thus,

$$\frac{x_{cp}}{D} = \frac{\frac{x_{cp0}}{D} C_{NSB} + \frac{x_c}{D} C_{NV}}{C_N} \quad (10)$$

For convenience, the alternative formulations are summarized in the table below.

CANDIDATE METHODS

$$C_N = C_{NSB} + C_{NV}$$

$$\frac{x_{cp}}{D} = \frac{\frac{x_{cp0}}{D} C_{NSB} + \frac{x_c}{D} C_{NV}}{C_N}$$

<u>Method</u>	<u>C_{NSB}</u>	<u>C_{NV}</u>
A	$\frac{C_{N\alpha}}{2} \sin 2\alpha \cos \frac{\alpha}{2}$	$c_{d_c} \frac{A_p}{A_{ref}} \sin^2 \alpha$
B	$C_{N\alpha} \sin \alpha$	$\left(c_{d_c} \frac{A_p}{A_{ref}} - C_{N\alpha} \right) \sin^2 \alpha$

For the comparisons with data the methods will use a common data base for $C_{N\alpha}$ and x_{cp_0} (described next) and the same relation for c_{d_c} (Figure 14). Figure 14 is adapted from Reference 13, with the irregular behavior of c_{d_c} in the region of $M_c \approx 1$ replaced with the faired curve shown. For the comparisons to be shown, the branch of the curve for turbulent flow for $M_c < .5$ has been used.

5.3 Data Base for $C_{N\alpha}$ and x_{cp_0}

A literature survey was made to identify existing data for these quantities. The search was limited to data for bodies with pointed tangent-ogive noses. The table below summarizes the results for $C_{N\alpha}$. The situation for x_{cp_0} is very similar. Examination of this table reveals that the data base of Reference 14 very nearly covers the ranges of interest of l_N/D , l_A/D and M_∞ , and that none of the other data bases extend the coverage in any significant way. The data base of Reference 14 was therefore selected for use in this study. To assess the level of agreement among the data bases where there is overlap, a series of comparisons were made. Figures 15 and 16 are samples of those comparisons for $C_{N\alpha}$ and x_{cp_0} , respectively, for the data of References 13 and 14. On the basis of these and the other comparisons not shown, it appears that the data from the different sources are generally within a band of about 10% for $C_{N\alpha}$ and 0.25 for x_{cp_0}/D .

These discrepancies obviously limit the ultimate accuracy achievable by any of the methods being considered.

DATA BASES FOR $C_{N\alpha}$ FOR BODIES WITH POINTED TANGENT-OGIVE NOSES

Ranges of Parameters Covered

<u>References</u>	<u>ℓ_N/D</u>	<u>ℓ_A/D</u>	<u>M_∞</u>
13	1.5, 2.5, 3.5	6-18*	0.8-1.2
	2.5, 3.0, 3.5, 4.0	4-10	1.5-3.0
14	0.5, 1.5, 2.5, 3.5	6-18	0.8-4.0
15	3, 5, 7	0-10	3-6.28
16**	2, 3, 4	0	2-4.5
17	2.84	0-11	1.36-4
18	1, 2.4	4, 8	0.6-1.5

5.4 Comparisons with Data

To evaluate which of the two methods previously outlined is most accurate, predictions were made for various combinations of parameters for bodies with pointed tangent-ogive noses for which there are experimental data. These predictions are compared to the data in Figures 17-29. Each of these figures is for a particular combination of ℓ_N/D , ℓ_A/D and M_∞ ; part (a) of each presents the comparison for C_N , part (b) for x_{cp}/D . The following configurations are investigated:

*For $\ell_N/D = 1.5$, data exist for $6 \leq \ell_A/D \leq 20$.

**Calculated using 3-D Method of Characteristics.

$\frac{\ell_N}{D}$	$\frac{\ell_A}{D}$	M_∞	Figure No.
1.5	13	0.8	17
↓	↓	1.2	18
↓	↓	2.0	19
2.5	7	1.2	20
↓	↓	2.0	21
↓	13	0.8	22
↓	↓	1.2	23
↓	↓	2.0	24
3.0	3.667	1.6	25
↓	↓	4.63	26
3.5	7	0.9	27
↓	↓	1.2	28
↓	↓	2.0	29

Examination of the comparisons for C_N in these figures reveals that the data are best predicted by Method B, and that the discrepancy between that method and the data is generally less than 10%. The only exception to this observation is for the high- α end of the data for $M_\infty = 0.8$ in Figure 17(a). For this case, there is the possibility that the data contain the effects of asymmetric vortex shedding, an effect clearly not accounted for in the simple methods considered here. Note that even in this case, Method B is closer to the data than Method A.

With respect to the location of the center of pressure, the agreement with data of the predictions is considerably more variable. There is no clear advantage for any of the methods over the others, so for consistency, Method B is selected for

use here as well as for C_N . Figures 17 through 29 show that the prediction of Method B for x_{cp} is within $0.6D$ of the measured location for nearly all of the cases considered, but the discrepancy is up to two to three times that level in the cases of Figures 17 and 18. As for C_N , however, in these cases of lowest accuracy, Method B is still superior to Method A.

5.5 Conclusions

The following formulations (used with the data base of Reference 14 and the c_{dc} curve of Figure 14) yield predictions of C_N and x_{cp}/D that are generally within 10% and 0.6, respectively, of measurements over the ranges of parameters shown:

$$C_N = C_{N_\alpha} \sin \alpha + \left(c_{dc} \frac{A_p}{A_{ref}} - C_{N_\alpha} \right) \sin^2 \alpha \quad (11)$$

$$\frac{x_{cp}}{D} = \frac{\frac{x_{cp0}}{D} (C_{N_\alpha} \sin \alpha) + \frac{x_c}{D} \left(c_{dc} \frac{A_p}{A_{ref}} - C_{N_\alpha} \right) \sin^2 \alpha}{C_N} \quad (12)$$

$$0.5 \leq \ell_N/D \leq 3.5$$

$$6 \leq \ell_A/D \leq 18$$

$$0.8 \leq M_\infty \leq 4.0$$

$$0 \leq \alpha \leq 45^\circ$$

These ranges are set by the data base of Reference 14. It is estimated that the small extrapolations necessary to cover the complete parameter space of interest can probably be made without appreciable loss of accuracy.

6. CONCLUDING REMARKS

At the end of the third-year's work, the following remarks can be made:

1. For $M_\infty = 1.2$, $C_{NF}(B)$ appears to be a fairly strong function of λ for $0 \leq \lambda \leq 1/2$, but it is only a weak function of λ for $1/2 \leq \lambda \leq 1$.

2. For cross flow Mach numbers greater than 0.5, the local properties of the flow field about a body have a very strong influence on $C_{NF}(B)$ resulting in the possibility of large control cross-coupling effects.

3. The variation of q_ℓ and M_ℓ around a body alone for $M_c > .5$ will have to be taken into account for correlation of center-of-pressure data for the data base and for extrapolating from the data base to other configurations using the α_{eq} concept.

4. The simplest version of the cross flow drag method appears to be capable of predicting body-alone normal force and center-of-pressure location to within 10% and 0.6 diameters respectively provided the vortex shedding is symmetric.

REFERENCES

1. Nielsen, J.N., Hensch, M.J., and Smith, C.A.: A Preliminary Method for Calculating the Aerodynamic Characteristics of Cruciform Missiles to High Angles of Attack Including Effects of Roll Angle and Control Deflections. NEAR TR 152, Nov., 1977.
2. Smith, C.A., and Nielsen, J.N.: Prediction of Aerodynamic Characteristics of Cruciform Missiles to High Angles of Attack Utilizing a Distributed Vortex Wake. NEAR TR 208, Jan., 1980.
3. Hensch, M.J., and Nielsen, J.N.: Triservice Program for Extending Missile Aerodynamic Data Base and Prediction Program Using Rational Modeling. Interim Report for Period June 16, 1980 to June 15, 1981. NEAR TR 249, Sept., 1981.
4. Hensch, M.J., and Nielsen, J.N.: Triservice Program for Extending Missile Aerodynamic Data Base and Prediction Program Using Rational Modeling. Interim Report for Period June 16, 1981 to June 15, 1982. NEAR TR 282, Aug., 1982.
5. Hensch, M.J., and Nielsen, J.N.: The Equivalent Angle-of-attack Method for Estimating the Nonlinear Aerodynamic Characteristics of Missile Wings and Control Surfaces. AIAA Paper 82-1338, Aug., 1982.
6. Hoerner, S.F.: Fluid-Dynamic Drag. Published by the author. 1965.
7. Wardlaw, A.B., Baltakis, J.P., Solomon, J.M., and Hackerman, L.B.: An Inviscid Computational Method for Tactical Missile Configurations. NSWC TR 81-457.
8. Klopfer, G.H., Kuhn, G.D., and Nielsen, J.N.: Euler Solutions of Supersonic Wing-Body Interference at High Incidence Including Vortex Effects. AIAA Paper 83-0460. Jan., 1983.
9. Landrum, E.J., and Babb, C.D.: Wind-Tunnel Force and Flow-Visualization Data at Mach Numbers From 1.6 to 4.63 for a Series of Bodies of Revolution at Angles of Attack From -4° to 60° . NASA TM 78813. March, 1979.
10. Nielsen, J.N. and Goodwin, F.K.: Preliminary Method for Estimating Hinge Moments of All-Movable Controls. NEAR TR 268, March, 1982.
11. Ward, G.N.: Supersonic Flow Past Slender Pointed Bodies. Quar. J. Mech. & Appl. Math., Vol. 2, Pt. I, Mar., 1949, pp. 75-97.

REFERENCES (CONTINUED)

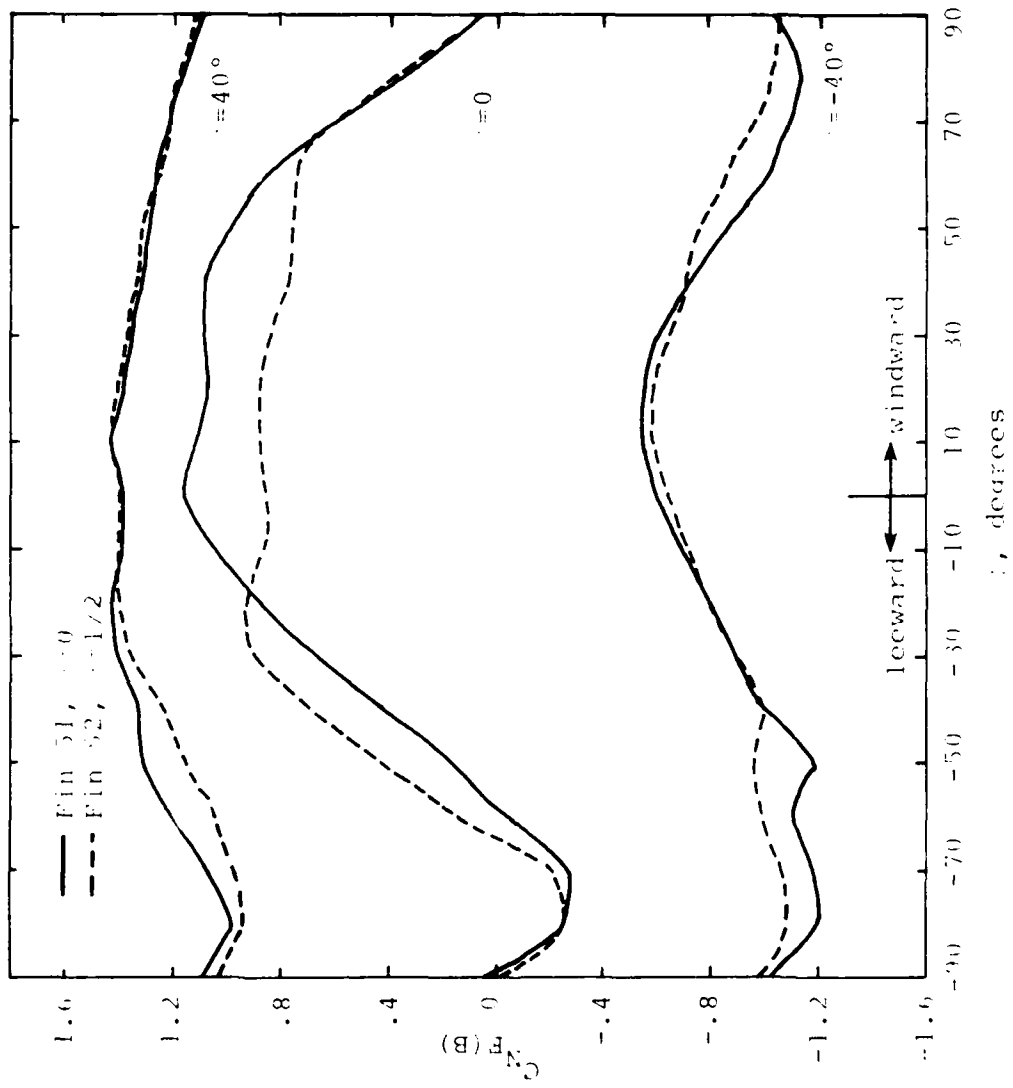
12. Jorgensen, L.H.: Prediction of Static Aerodynamic Characteristics for Slender Bodies Alone and With Lifting Surfaces to Very High Angles of Attack. NASA TR-474, Sept., 1977.
13. Aiello, G.F. and Bateman, M.C.: Aerodynamic Stability Technology for Maneuverable Missiles. Vol. I - Configuration Aerodynamic Characteristics. AFFDL-TR-76-55, Vol I, March, 1979.
14. Barth, H.: Die Normalkraft-, Druckpunkt- und Tangentialkraftcharakteristiken schlanker Bug-Zylinder-Konfigurationen im Machzahlbereich 0,8 bis 4,0. BMVg-FBWT 73-32, 1973.
15. Syvertson, C.A. and Dennis, D.H.: A Second-Order Shock-Expansion Method Applicable to Bodies of Revolution Near Zero Lift. NACA Report 1328, 1957.
16. Richardson, R.L. and Jenkins, B.Z.: Theoretical Analysis of the Flow Field Over a Family of Ogive Bodies - Vol. II - USAMICOM Report T-CR-77-5, Aug., 1979.
17. Buford, W.E.: The Effects of Afterbody Length and Mach Number on the Normal Force and Center of Pressure of Conical and Ogival Nose Bodies. JAS, Vol. 25, 1958, pp. 103-108.
18. Anderson, C.F. and Henson, J.R.: Aerodynamic Characteristics of Several Bluff Bodies of Revolution at Mach Numbers from 0.6 to 1.5. AEDC-TR-71-130, AFATL-TR-71-82, July, 1971.
19. Kruse, R.L., Keener, E.R., Chapman, G.T., and Claser, G.: Investigation of the Asymmetric Aerodynamic Characteristics of Cylindrical Bodies of Revolution with Variations in Nose Geometry and Rotational Orientation at Angles of Attack to 58° and Mach Number to 2. NASA TM 78533, Sept., 1979.
20. Jorgensen, L.H. and Nelson, E.R.: Experimental Aerodynamic Characteristics for a Cylindrical Body of Revolution with Various Noses at Angles of Attack from 0° to 58° and Mach Numbers from 0.6 to 2.0. NASA TM X-3128, Dec., 1974.
21. Landrum, E.J. and Babb, C.D.: Wind Tunnel Force and Flow Visualization Data at Mach Numbers from 1.6 to 4.63 for a series of Bodies of Revolution at Angles of Attack from -4° to 60°. NASA TM 78813, March, 1979.

Table 1.- Example of tabular output from data processing program for fin 42.

AR = 1.00 TR = 0.5 MACH = 2.5 D2 = 0 DEG

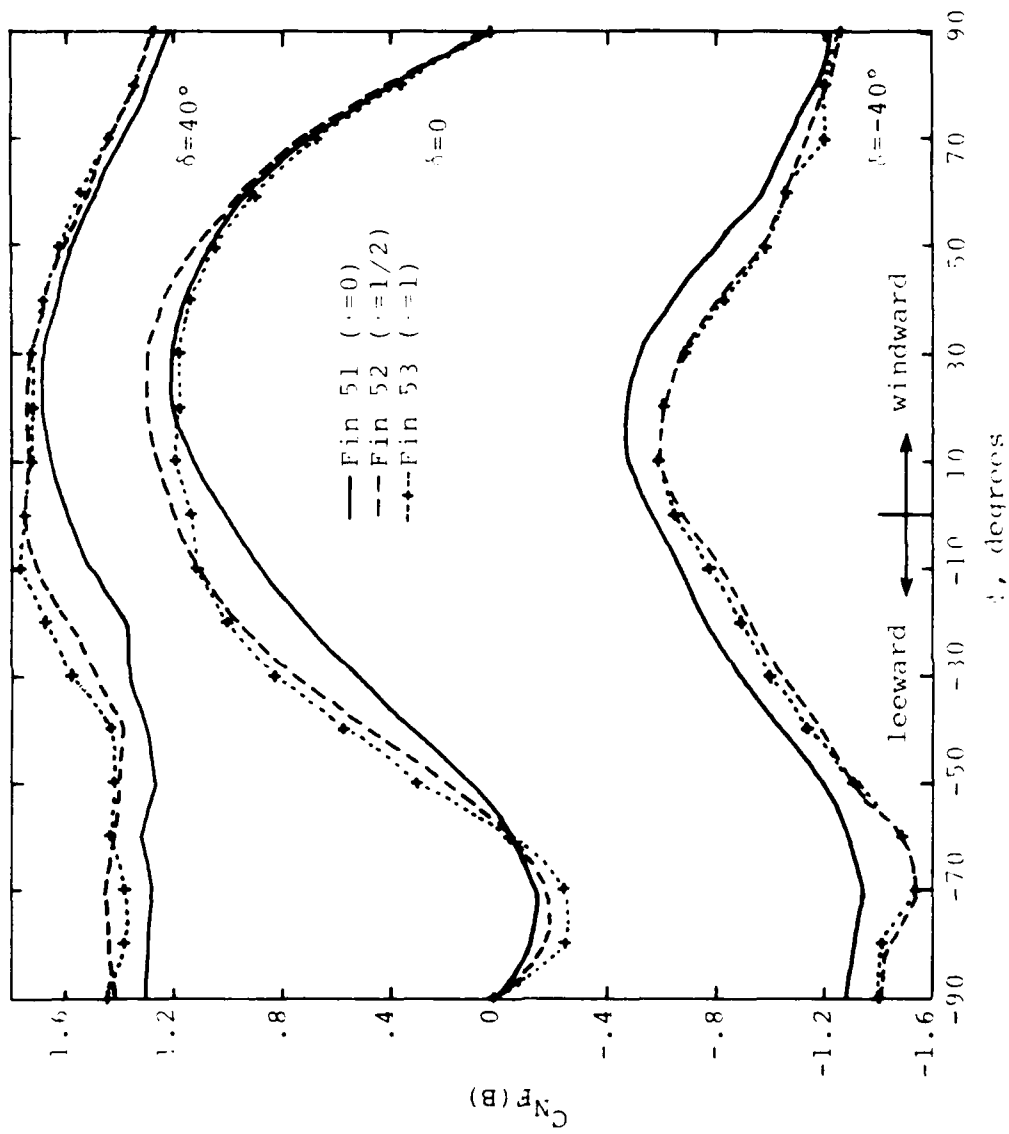
CNF(B) FOR ALPHAC = (DEG)

PHI, DEG	0	5	10	15	20	25	30	35	40	45
-90	0.000	0.000	0.000	0.000	0.000	0.000	0.000	0.000	0.000	0.000
-80	0.000	0.014	-0.033	-0.092	-0.080	-0.052	-0.021	-0.008	0.004	0.008
-70	0.000	0.030	-0.072	-0.115	-0.084	-0.044	-0.013	0.010	0.039	0.067
-60	0.000	0.053	-0.024	-0.045	-0.030	0.005	0.042	0.096	0.134	0.168
-50	0.000	0.078	0.047	0.020	0.042	0.097	0.161	0.217	0.260	0.300
-40	0.000	0.100	0.105	0.094	0.139	0.212	0.282	0.350	0.405	0.450
-30	0.000	0.123	0.173	0.183	0.253	0.341	0.432	0.514	0.585	0.647
-20	0.000	0.142	0.221	0.269	0.350	0.450	0.558	0.664	0.757	0.851
-10	0.000	0.154	0.260	0.349	0.442	0.555	0.682	0.807	0.936	1.062
0	0.000	0.162	0.285	0.383	0.503	0.635	0.774	0.929	1.095	1.254
10	0.000	0.161	0.306	0.419	0.544	0.683	0.848	1.032	1.221	1.401
20	0.000	0.159	0.316	0.441	0.562	0.707	0.889	1.090	1.306	1.498
30	0.000	0.146	0.301	0.429	0.553	0.699	0.875	1.093	1.319	1.517
40	0.000	0.130	0.272	0.390	0.514	0.664	0.832	1.036	1.266	1.505
50	0.000	0.109	0.230	0.336	0.446	0.580	0.731	0.914	1.119	1.365
60	0.000	0.086	0.178	0.263	0.353	0.456	0.584	0.731	0.899	1.104
70	0.000	0.058	0.122	0.181	0.244	0.319	0.411	0.516	0.630	0.774
80	0.000	0.023	0.059	0.088	0.116	0.152	0.196	0.249	0.304	0.370
90	0.000	0.000	0.000	0.000	0.000	0.000	0.000	0.000	0.000	0.000



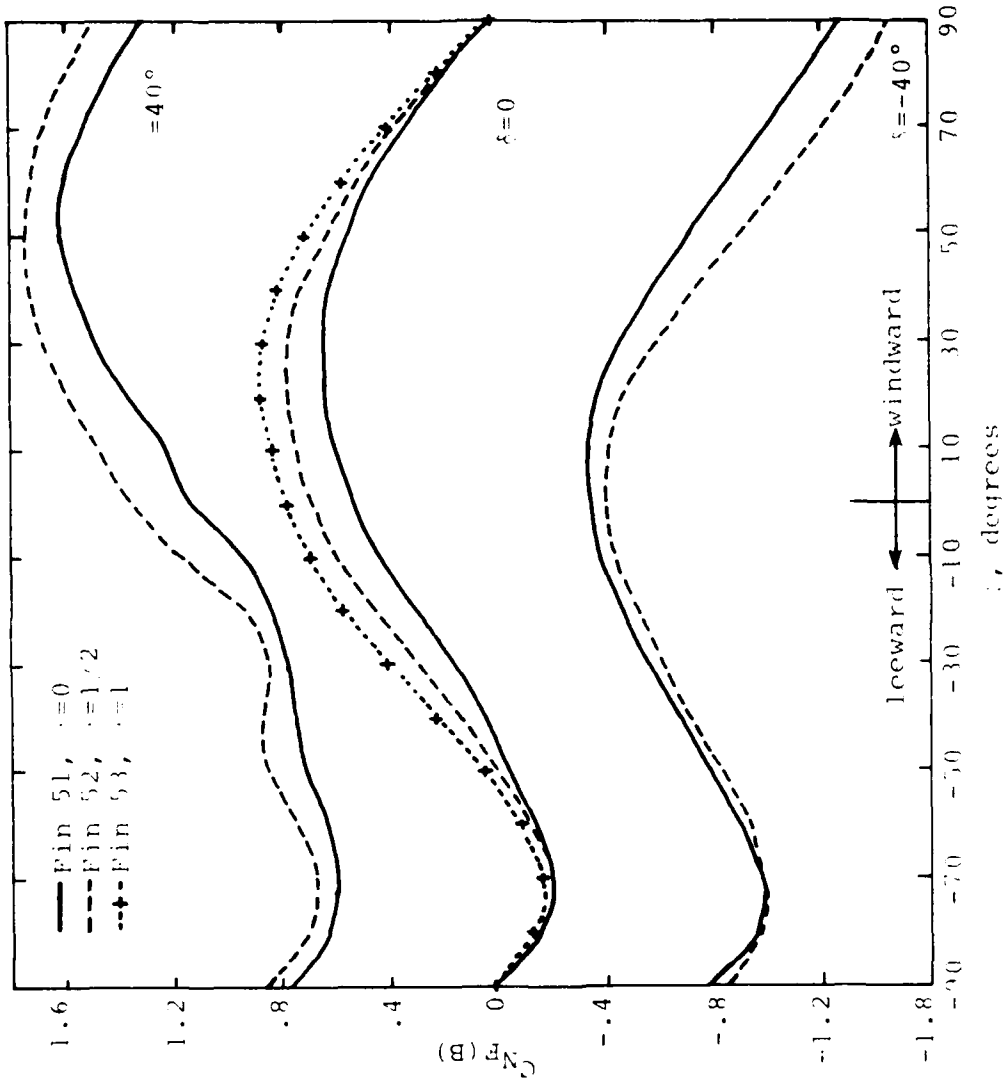
(a) $M_\infty = 0.8$

Figure 1.- Control effectiveness for aspect ratio 2 fins on a two-cylinder body at $\alpha_c = 20^\circ$.



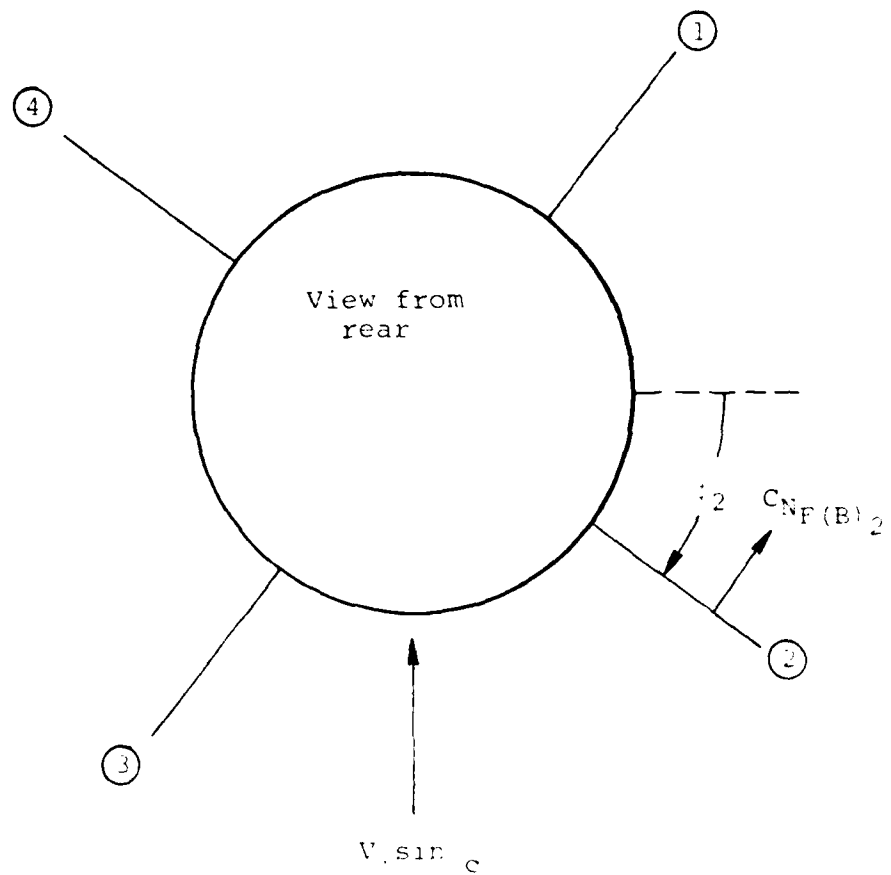
(b) $M_\infty = 1.2$

Figure 1.- Continued.



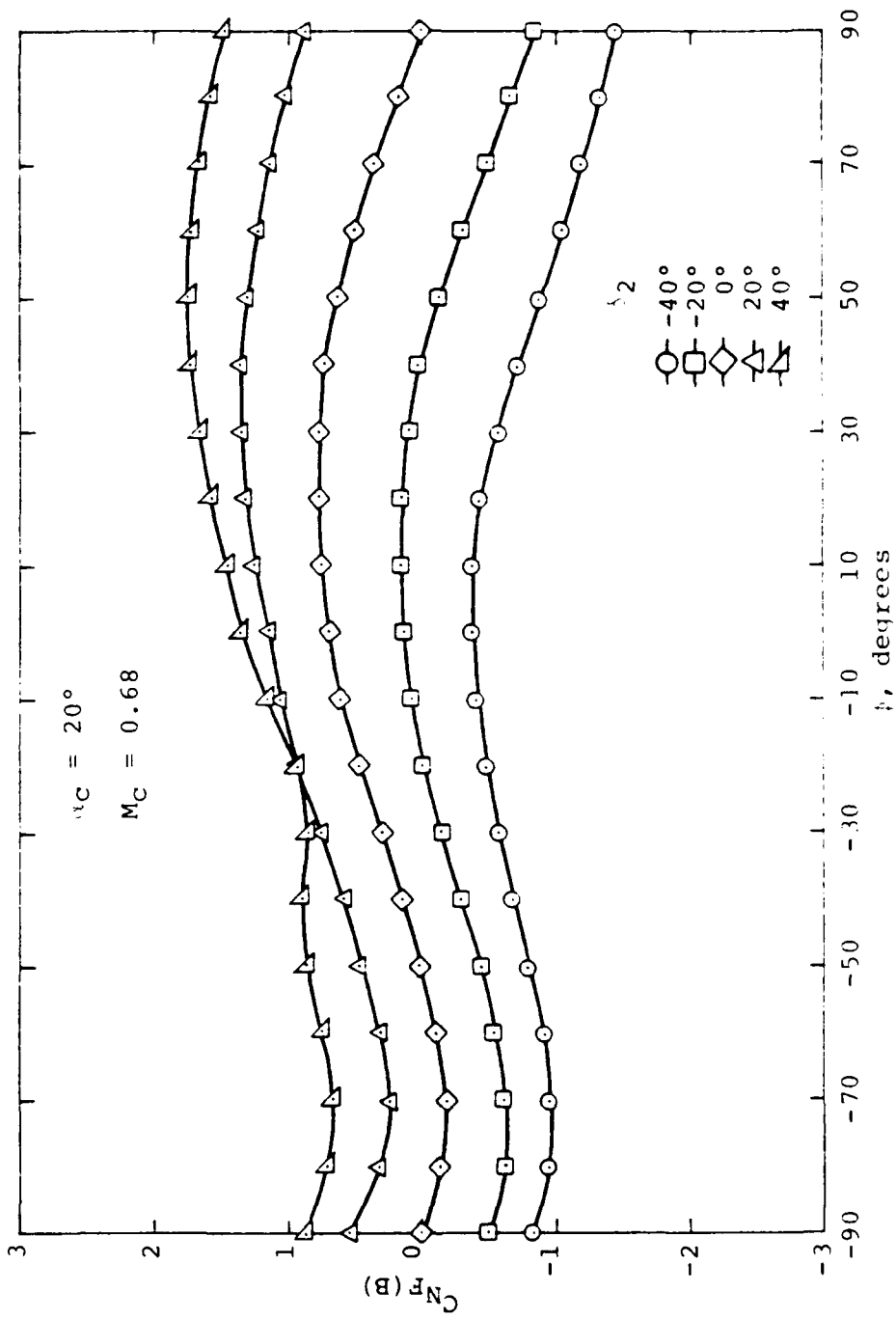
(*) $M_\infty = 2.0$

Figure 1.- Concluded.



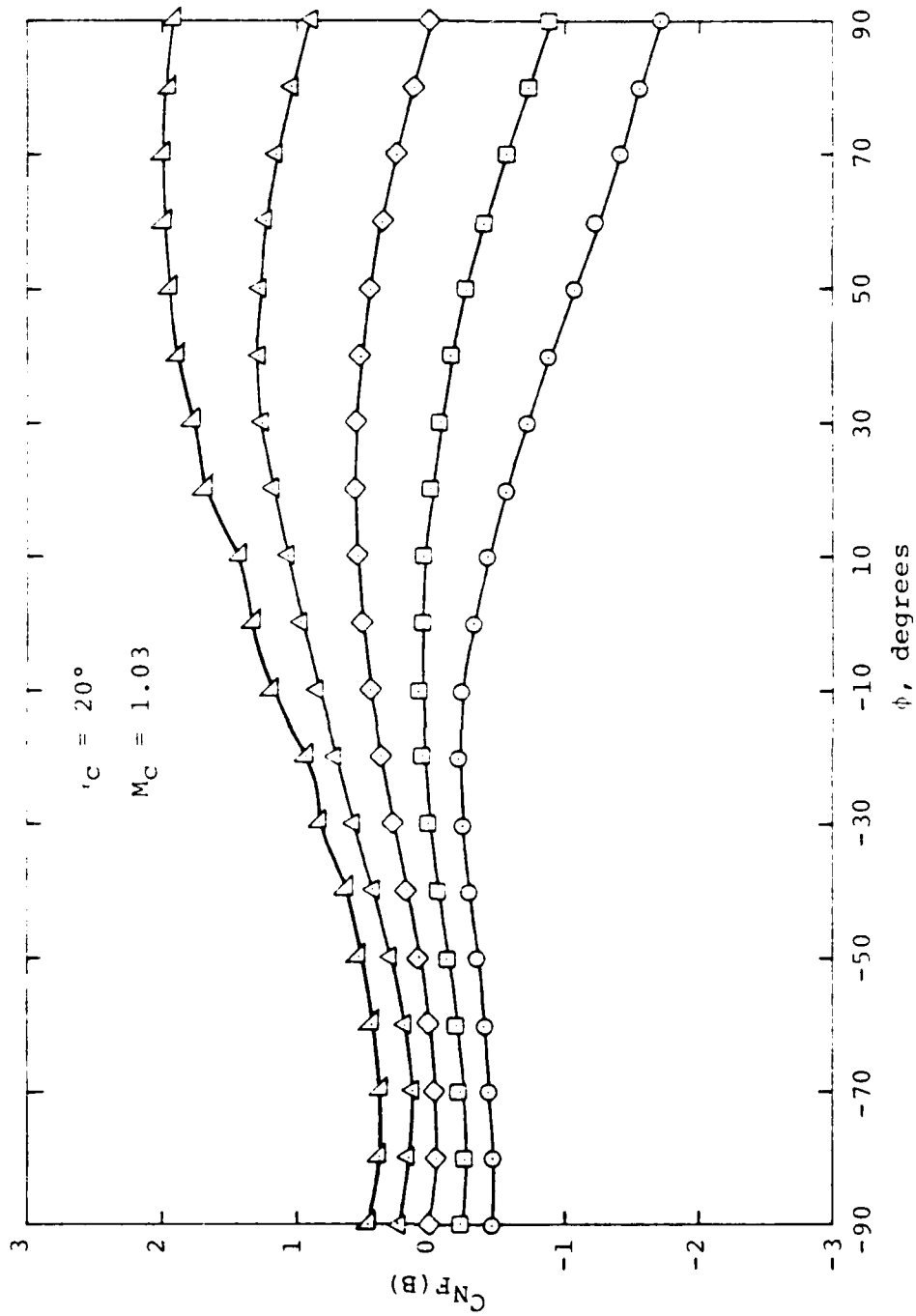
Note: Fin 2 is the deflecting fin. α is positive so as to produce a positive C_N in the direction shown.

Figure 2.- Fin sign conventions.



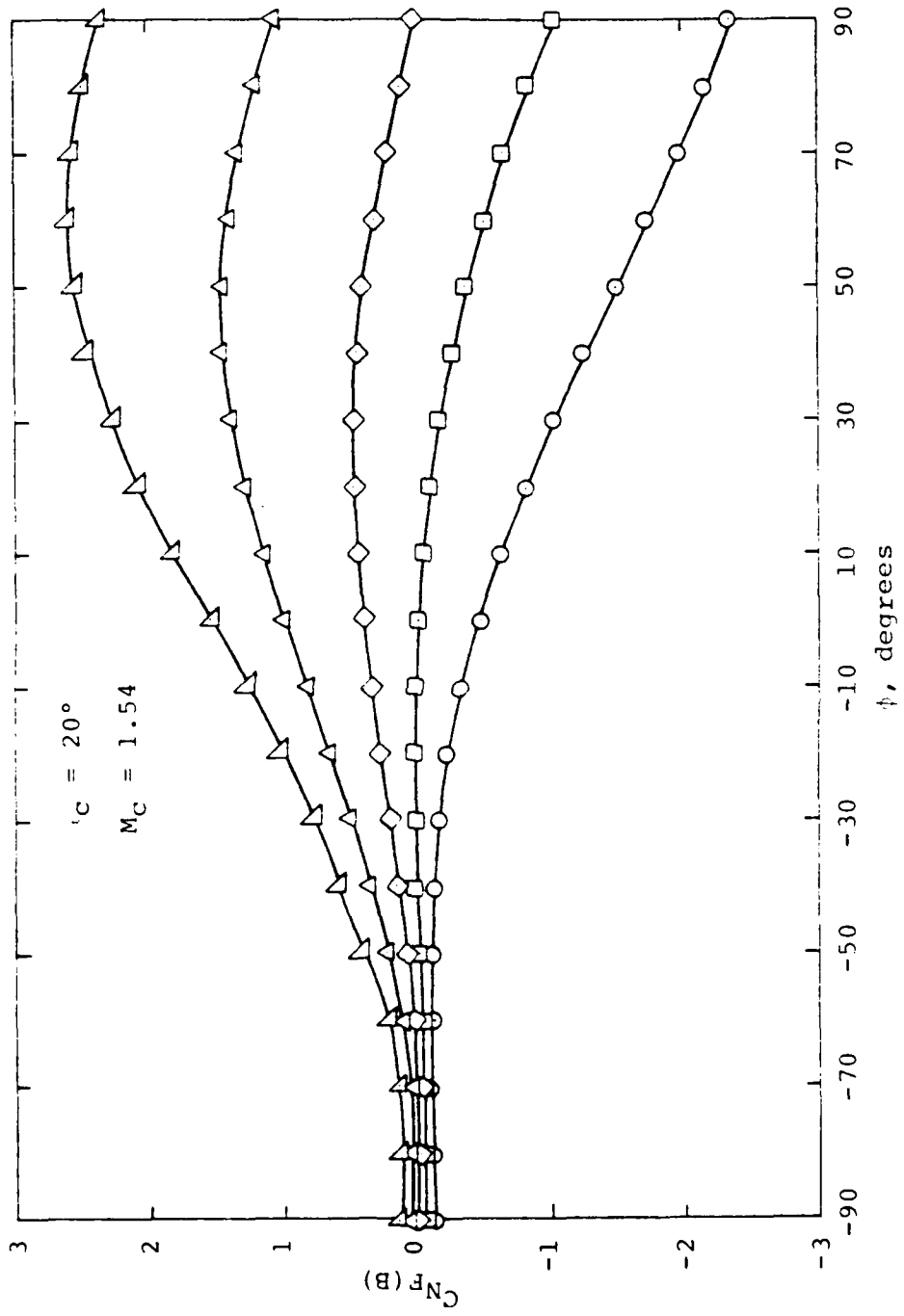
(a) $M_\infty = 2.0$

Figure 3.- Normal-force coefficient for deflected fin of $AR = 2$, $\lambda = 1/2$ (Fin 52).



(b) $M_\infty = 3.0$

Figure 3.- Continued.



(c) $M_c = 4.5$

Figure 3.- Concluded.

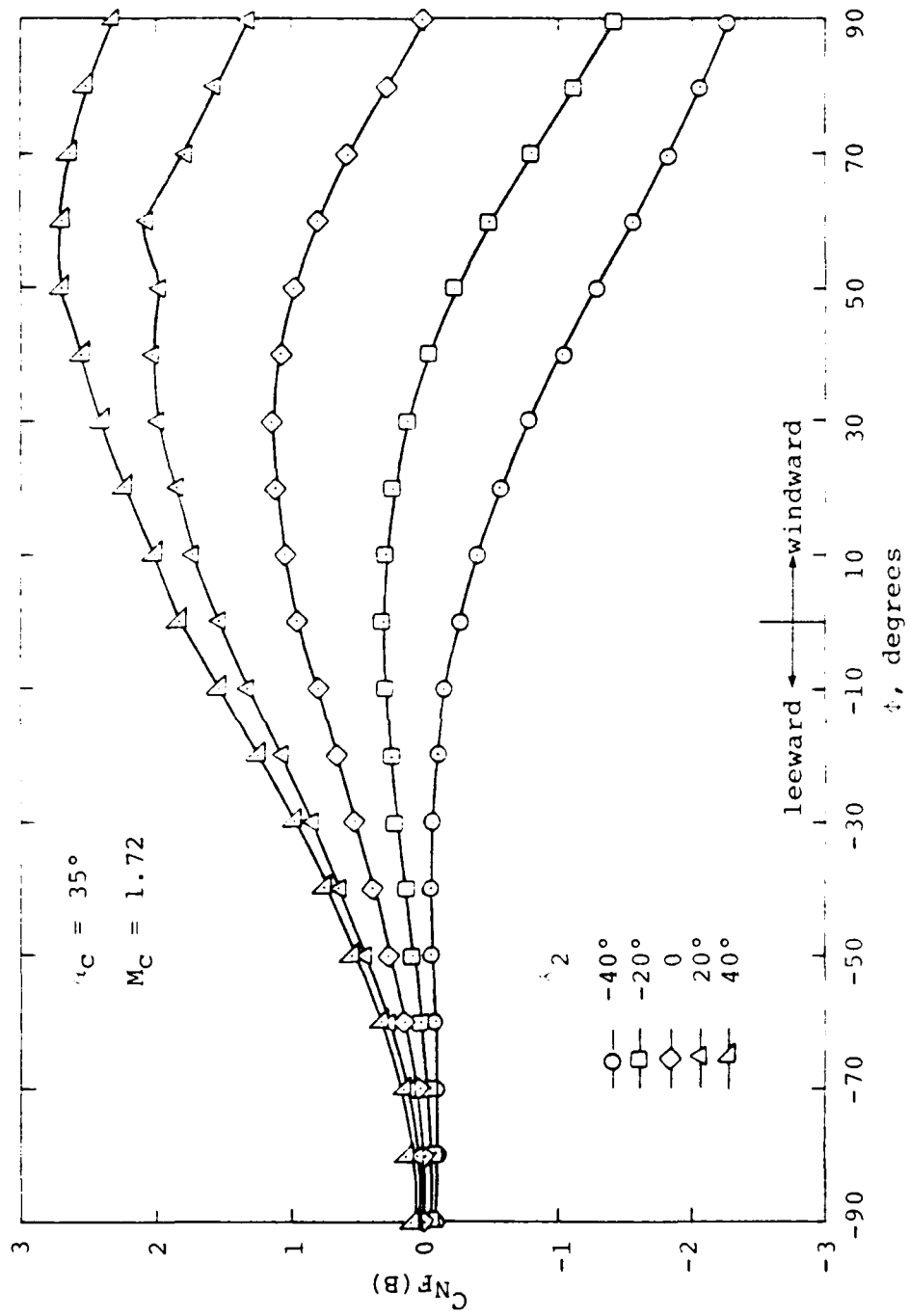


Figure 4.- Normal-force coefficient for deflected fin of AR = 2, $\alpha_C = 35^\circ$; $M_C = 1.72$ (Fin 52); $M_C = 3.0$, $\alpha_C = 35^\circ$ case.

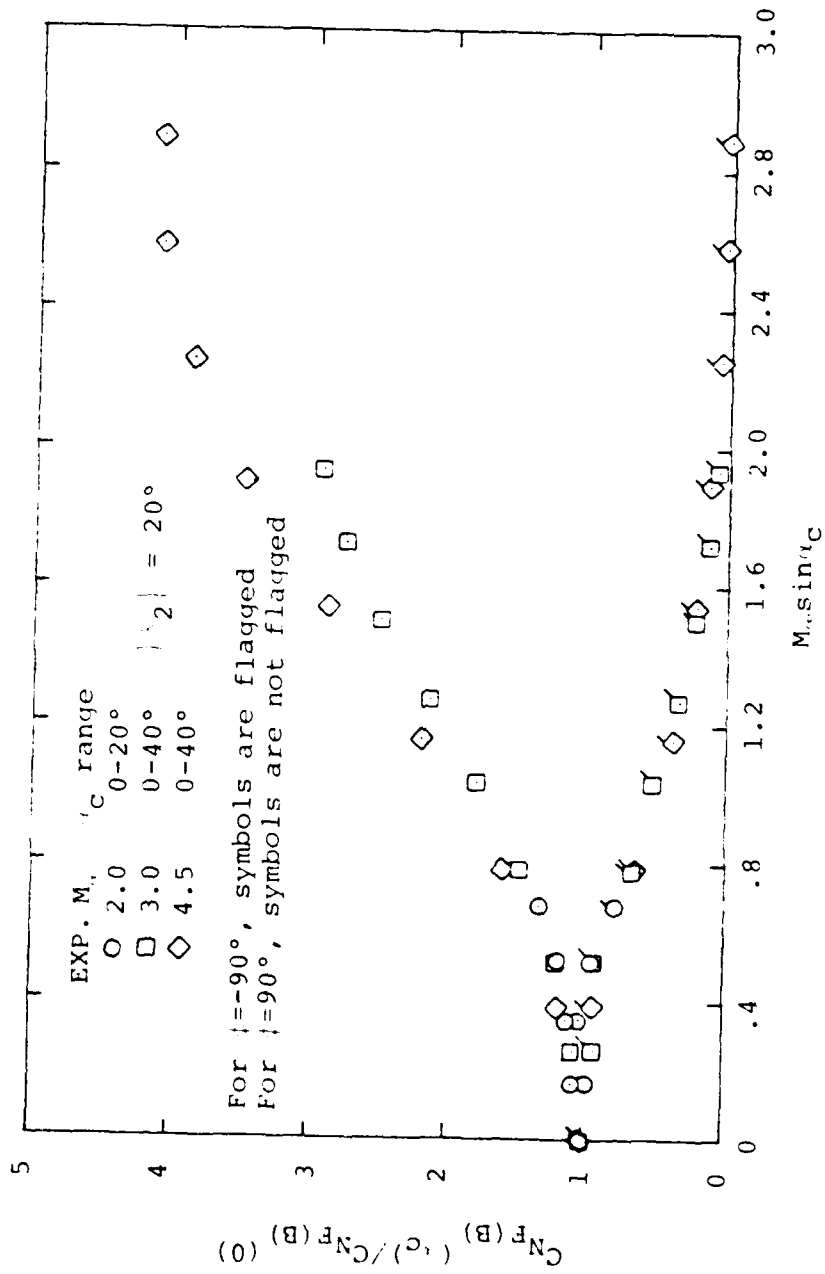
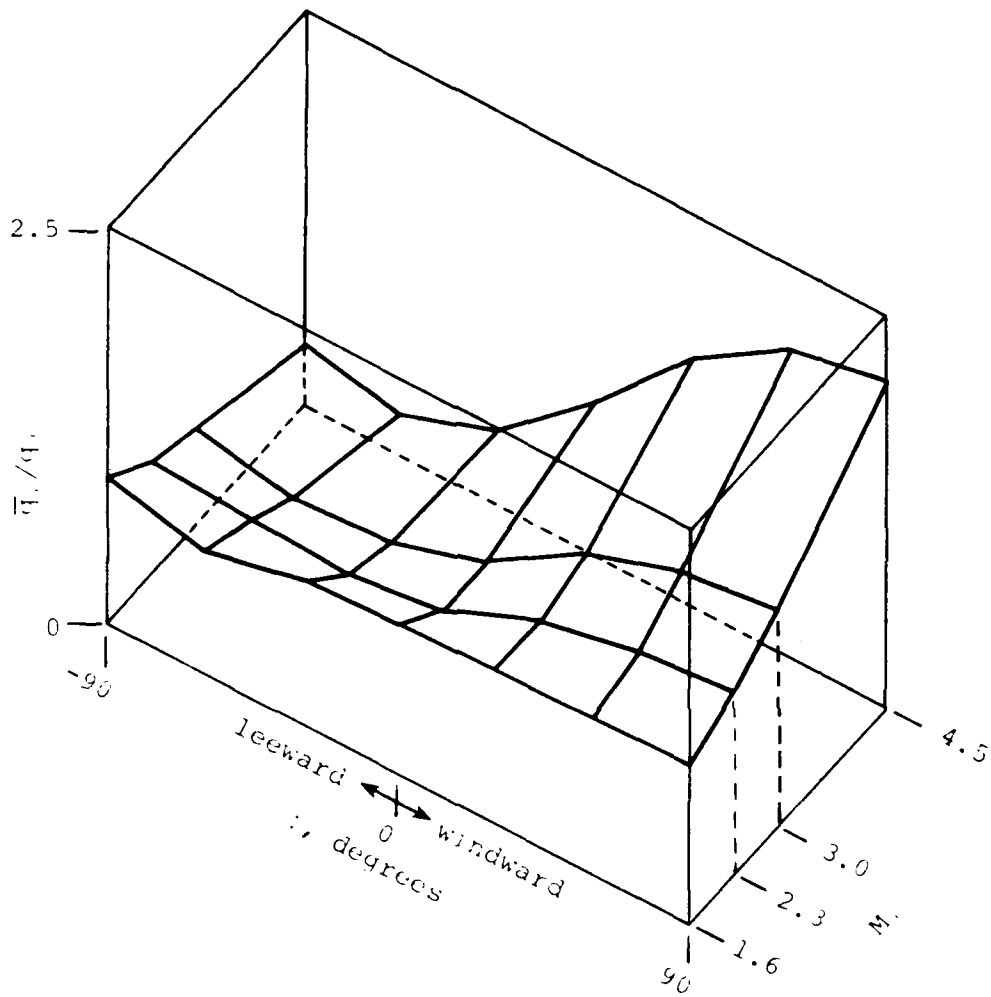
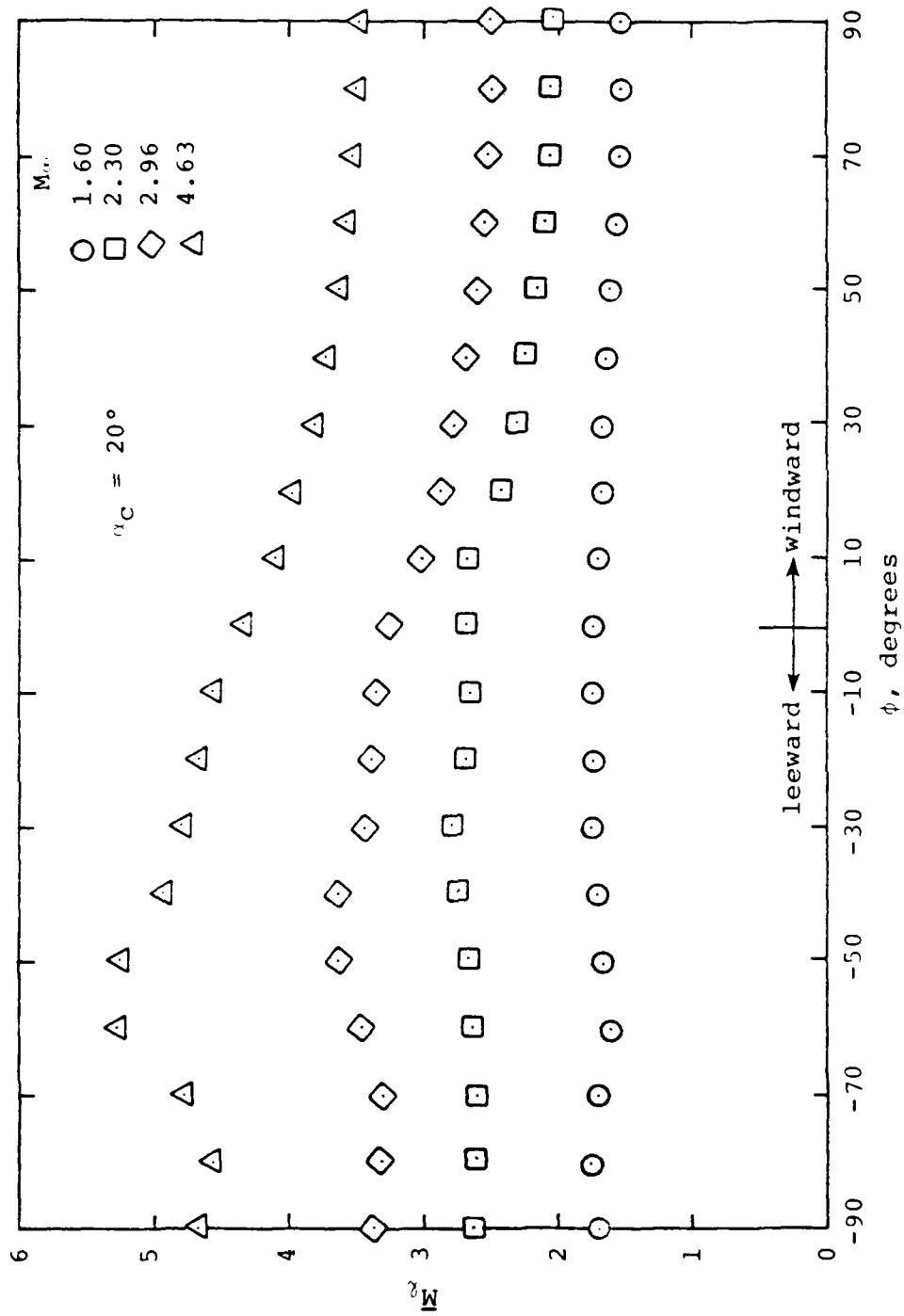


Figure 5.- Correlation of control effectiveness for leeward and windward fin positions.



(a) Average local dynamic pressure.

Figure 6.- Computed flow field properties 10 diameters aft of the nose tip of a 3-caliber-cone cylinder at 20° angle of attack; $a/s_m = 0.5$.



(b) Average local Mach number

Figure 6.- Concluded.

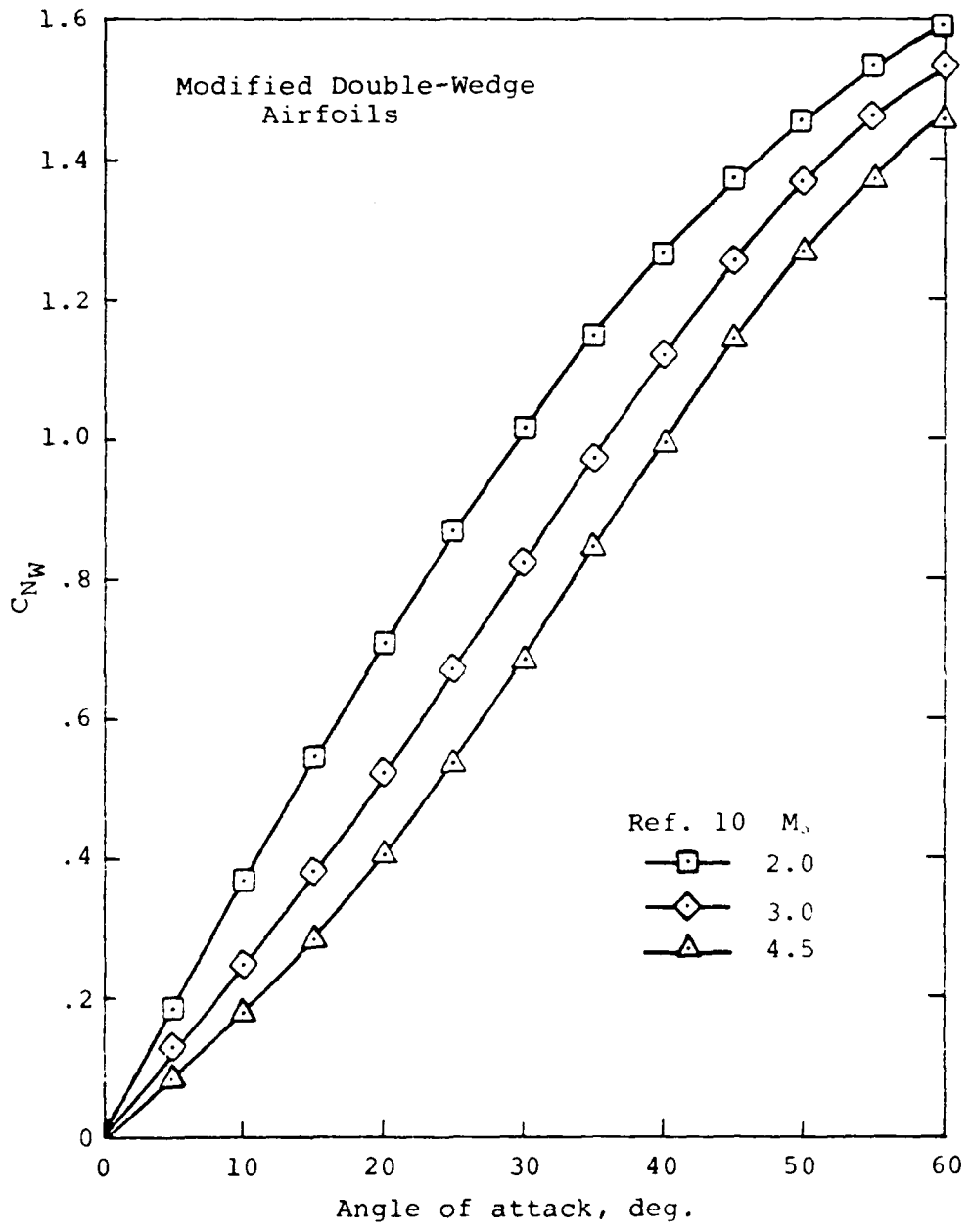


Figure 7.- Normal-force coefficient for $AR = 2$, $\lambda = 1/2$ clipped delta wing.

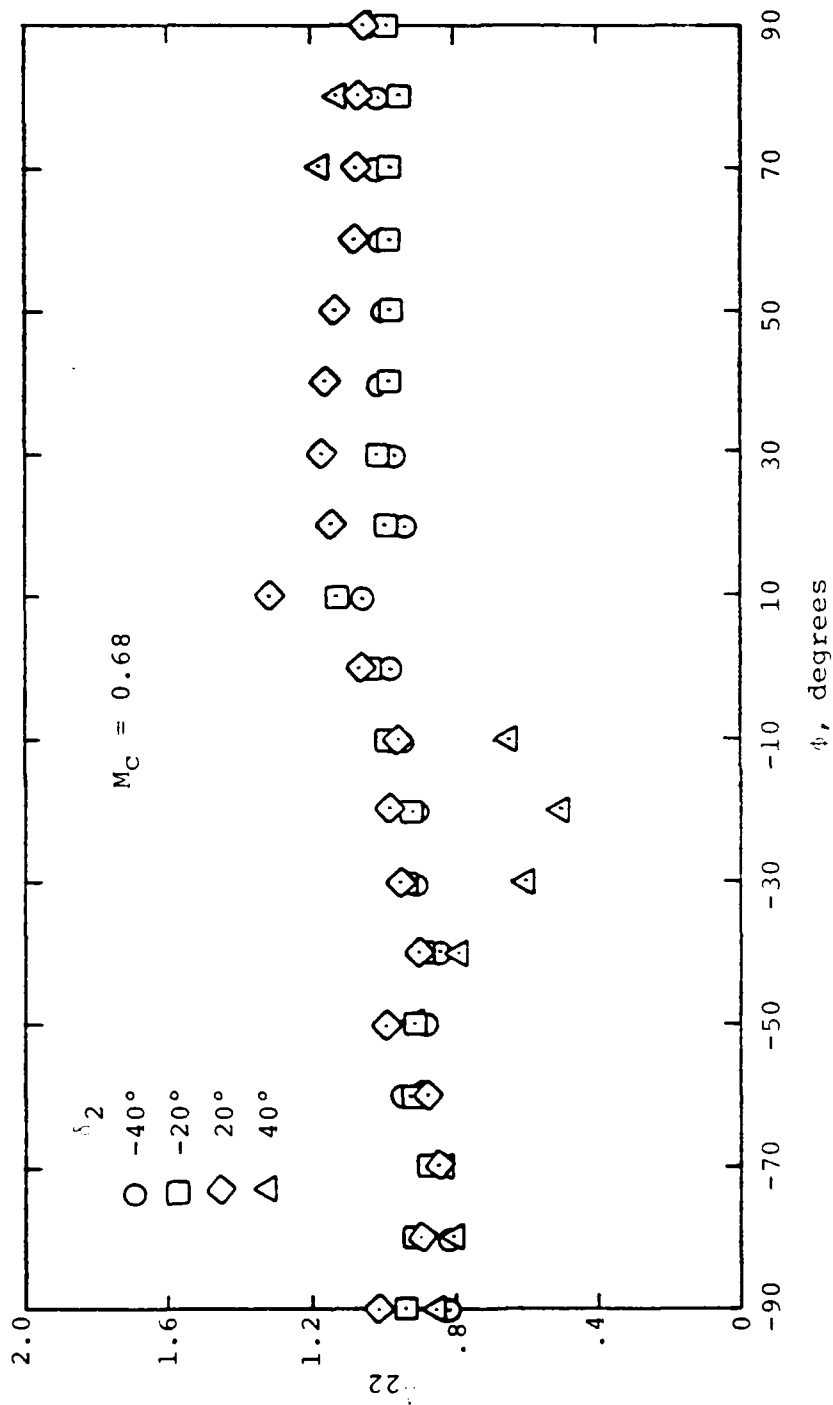
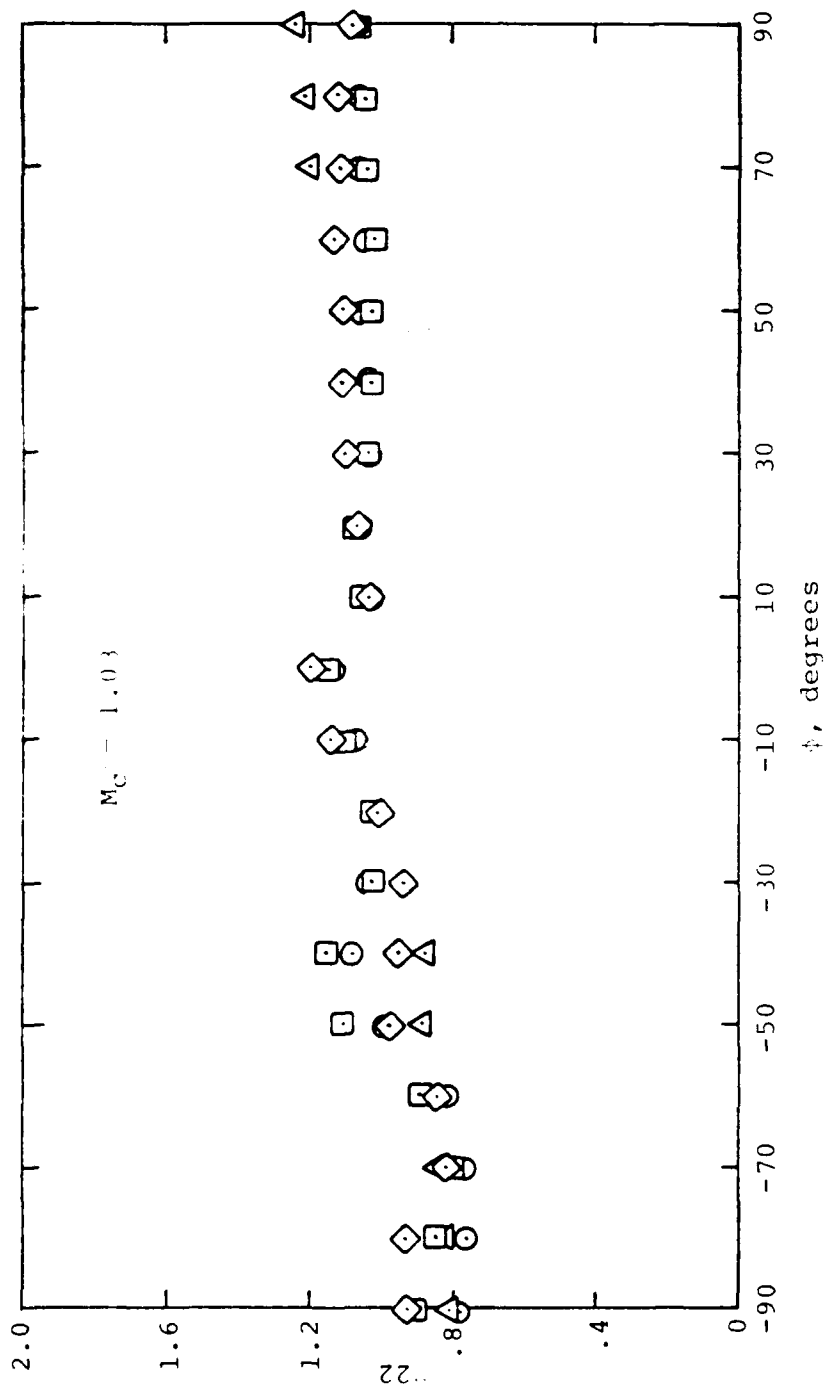
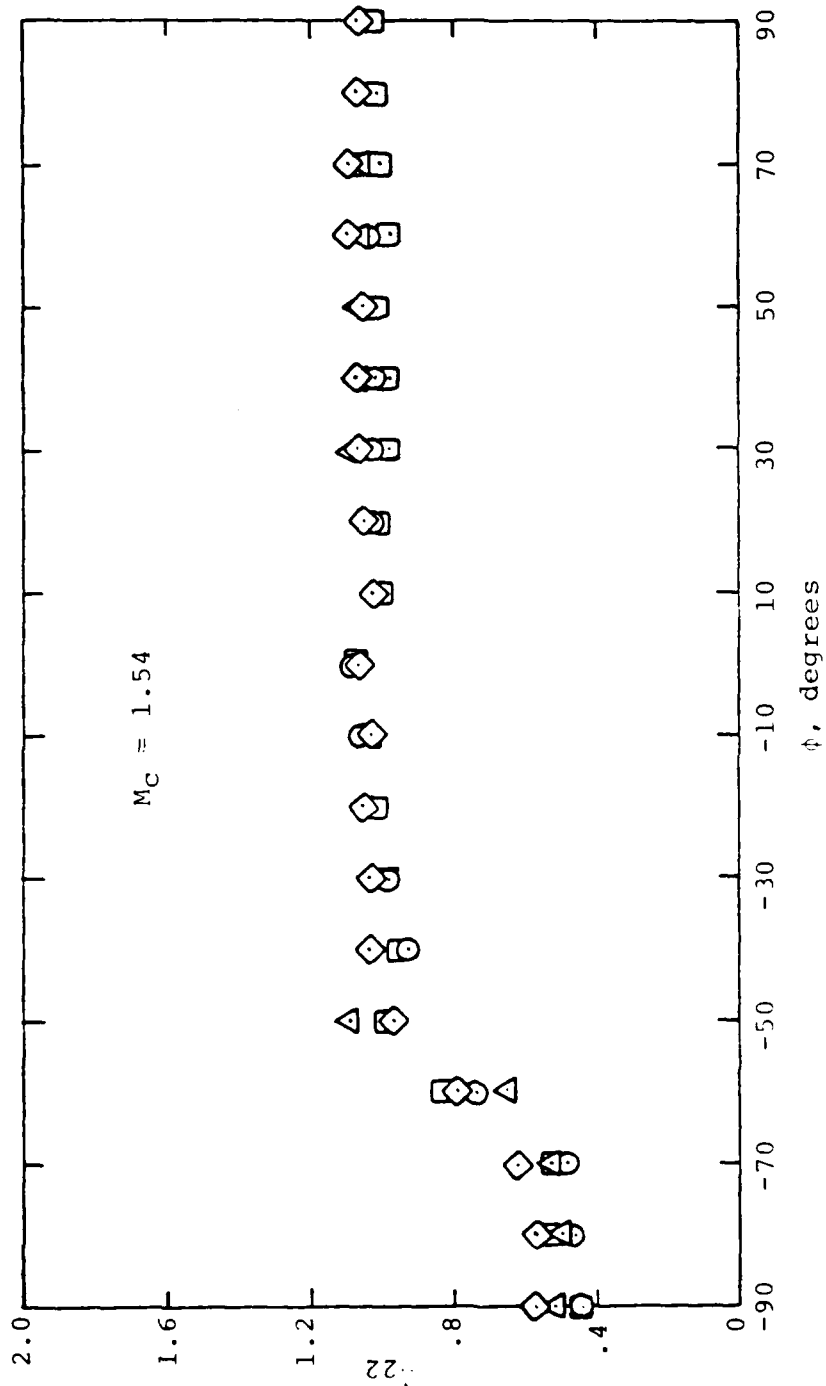


Figure 8.- Correlation of control fin effectiveness data of Figure 3; $\alpha_C = 20^\circ$.



(b) $M_{\infty} = 3.0$

Figure 8.- Continued.



(c) $M_n = 4.5$
 Figure 8.- Concluded.

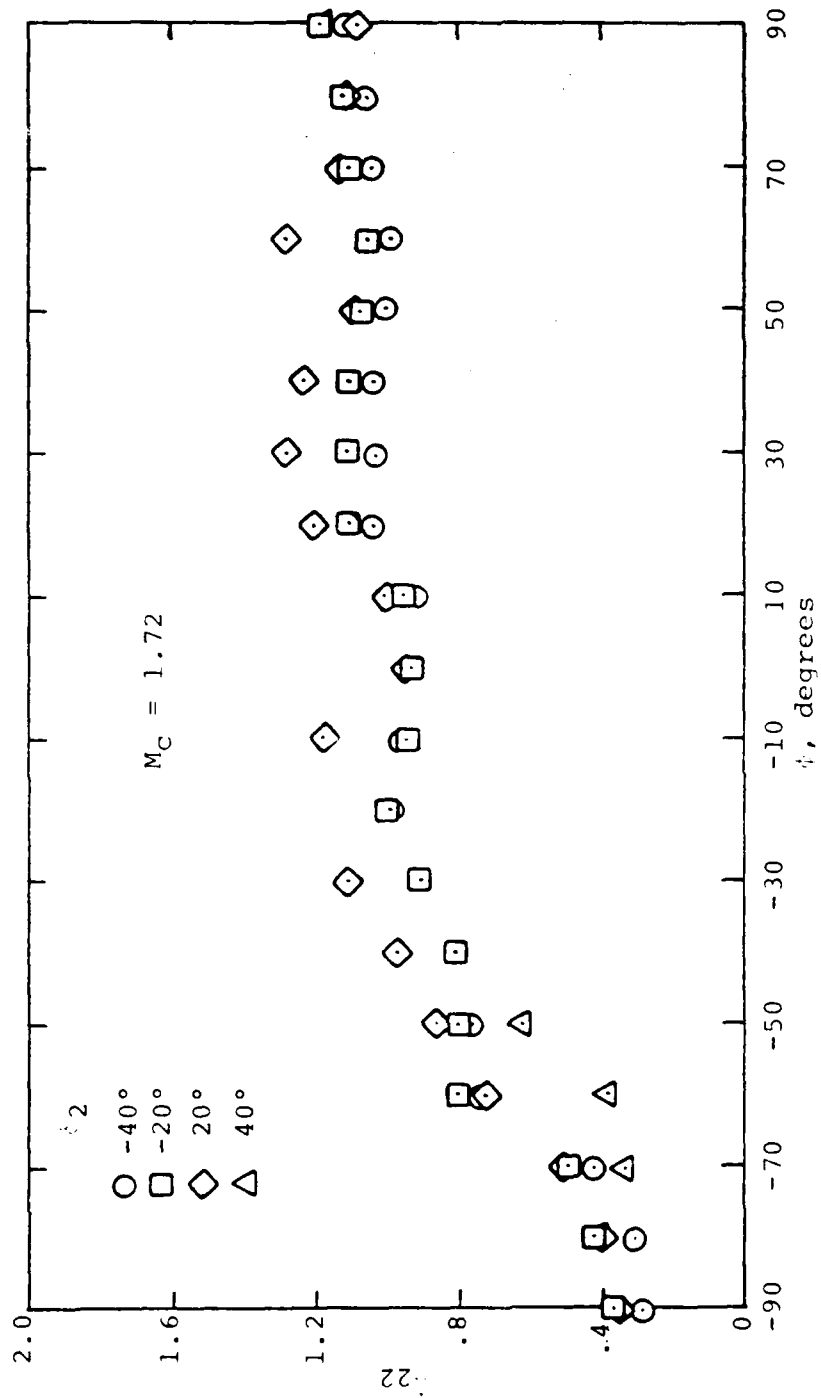


Figure 9.- Correlation of control fin effectiveness data of Figure 4; $M_c = 3.0$, $r_c = 35^\circ$.

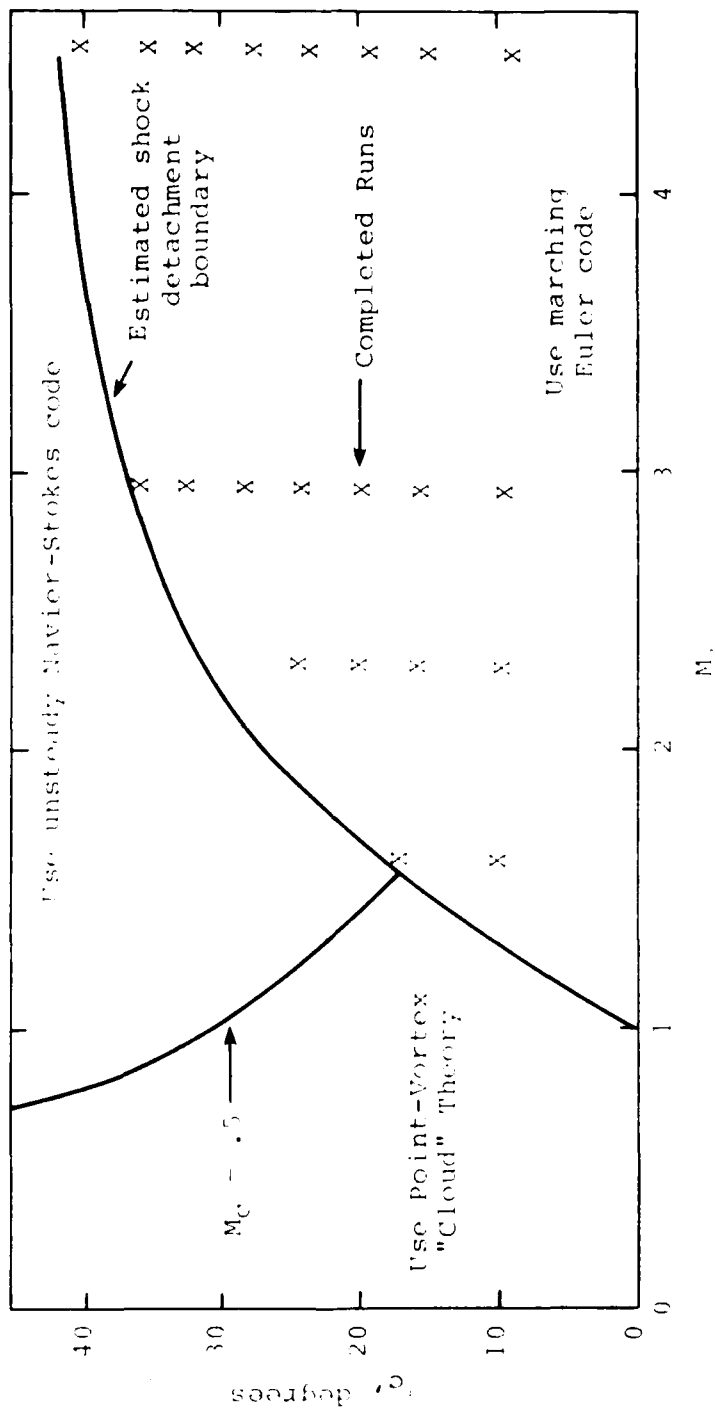


Figure 10.- Mach number/angle-of-attack domains for CFD code use.

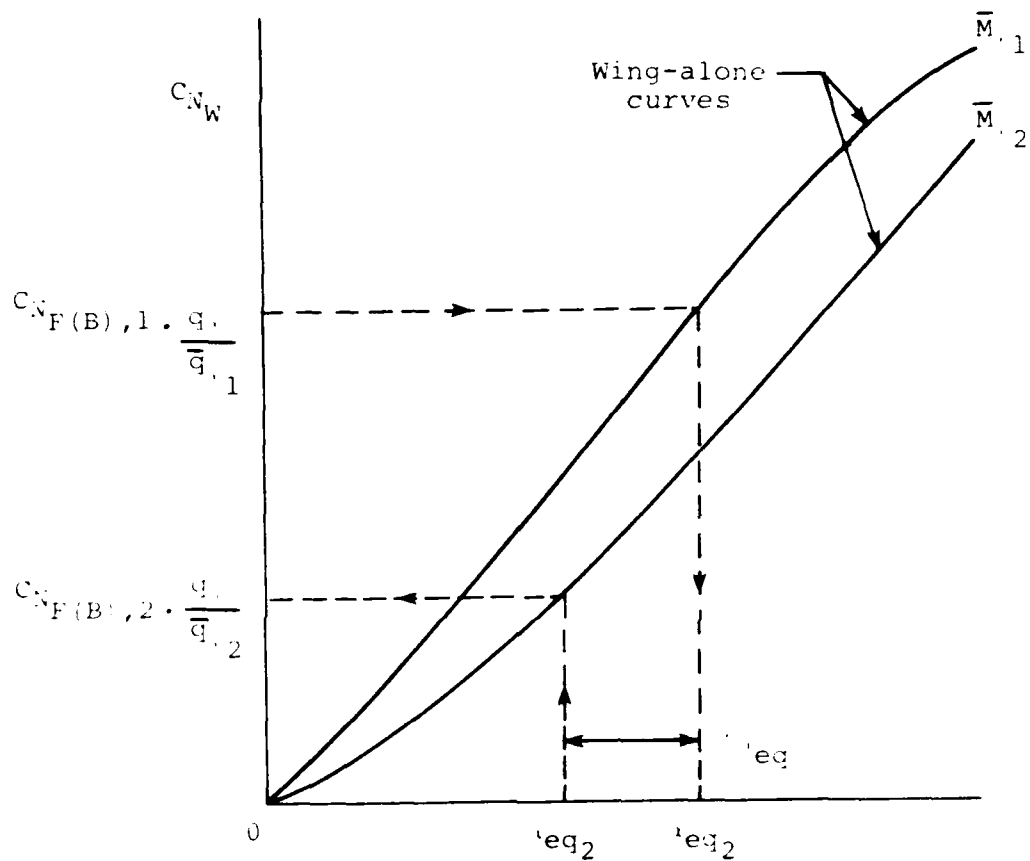
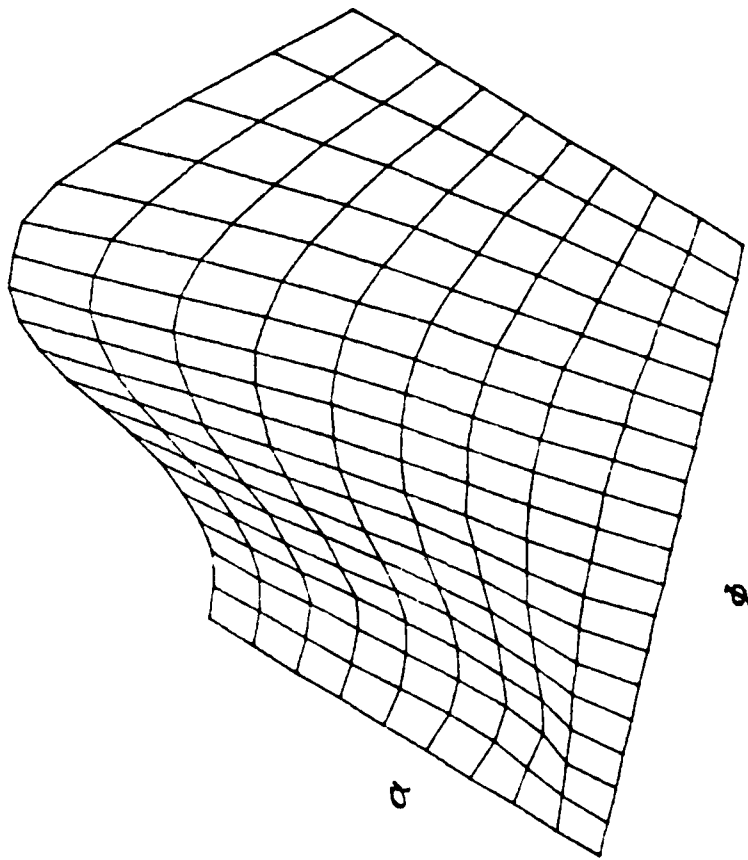


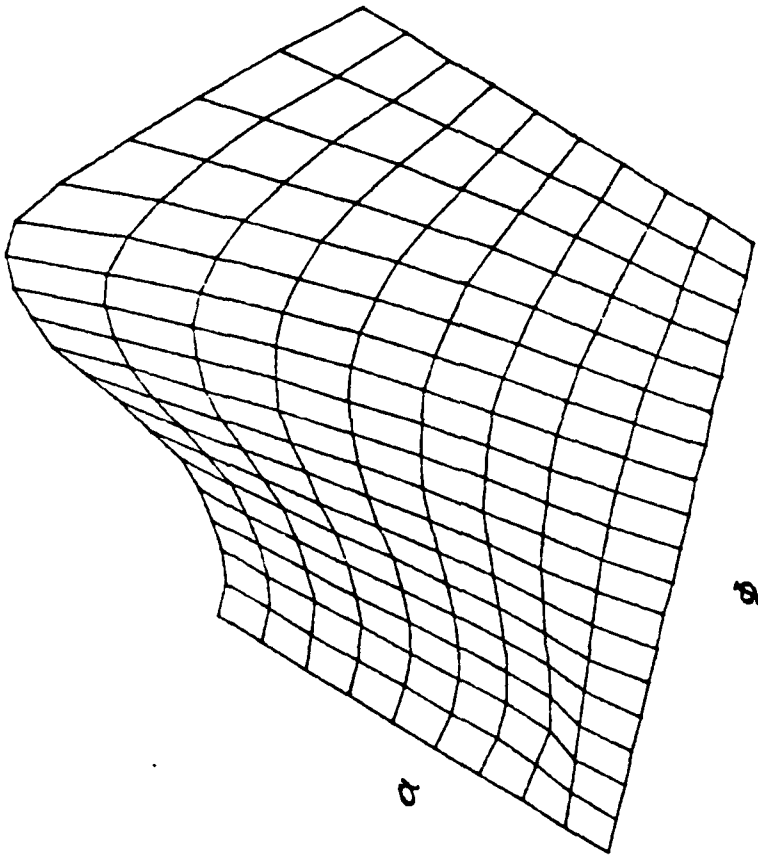
Figure 11.- Illustration of Δ_{eq} method as applied to extrapolation of fin-on-body data base.



FIN NORMAL-FORCE COEFFICIENT

(a) MACH = 2.5 AR = 1.00 TR = 0.5 D2 = 0. FIN 42

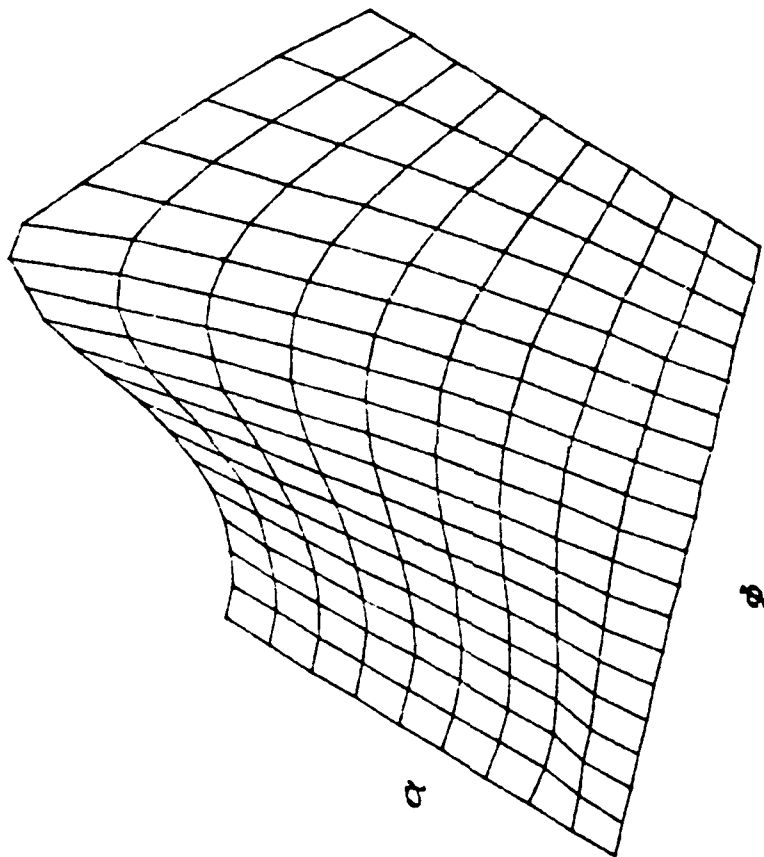
Figure 12.- Graphics display of fin normal-force coefficient.



FIN NORMAL-FORCE COEFFICIENT

(b) MACH = 3.0 AR = 1.00 TR = 0.5 D2 = 0. FIN 42

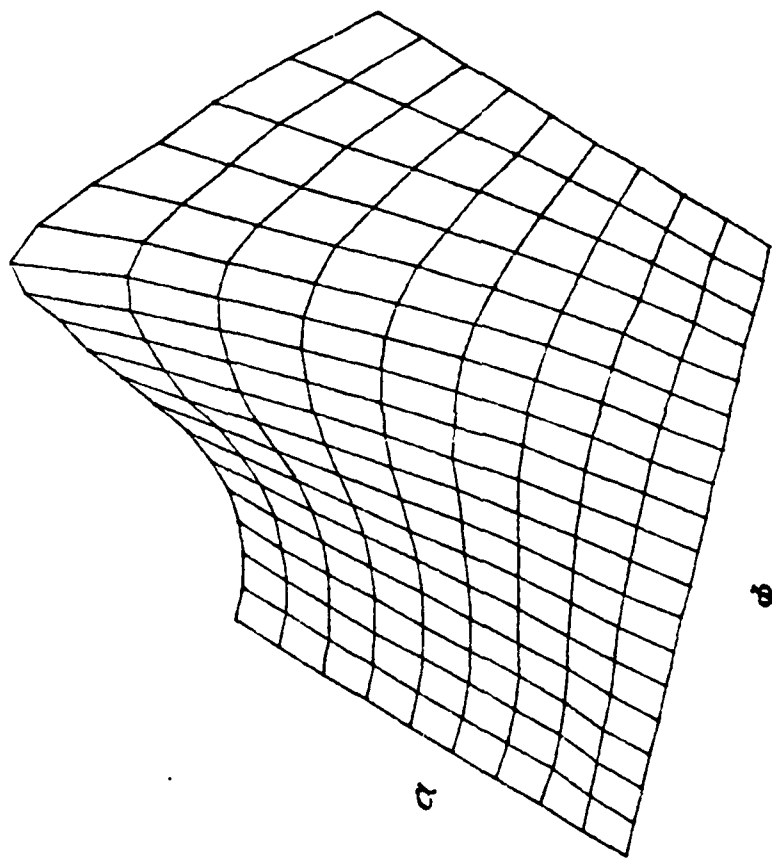
Figure 12.- (Continued).



FIN NORMAL-FORCE COEFFICIENT

(c) MACH = 3.5 AR = 1.00 TR = 0.5 D2 = 0. FIN 42

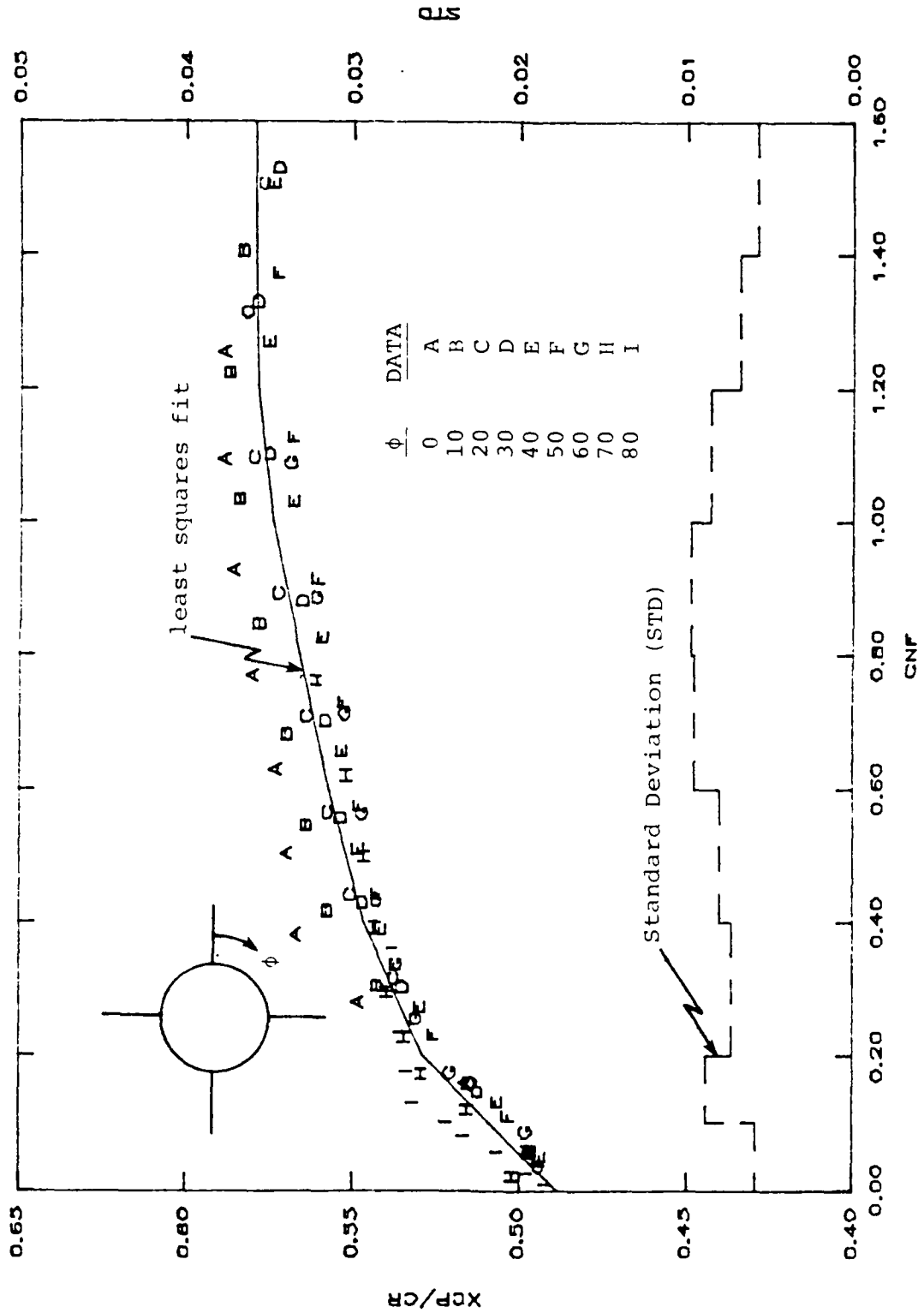
Figure 12.- (Continued).



FIN NORMAL-FORCE COEFFICIENT

(a) MACH = 4.5 AR = 1.00 TR = 0.5 D2 = 0. FIN 42

Figure 12. (Concluded).

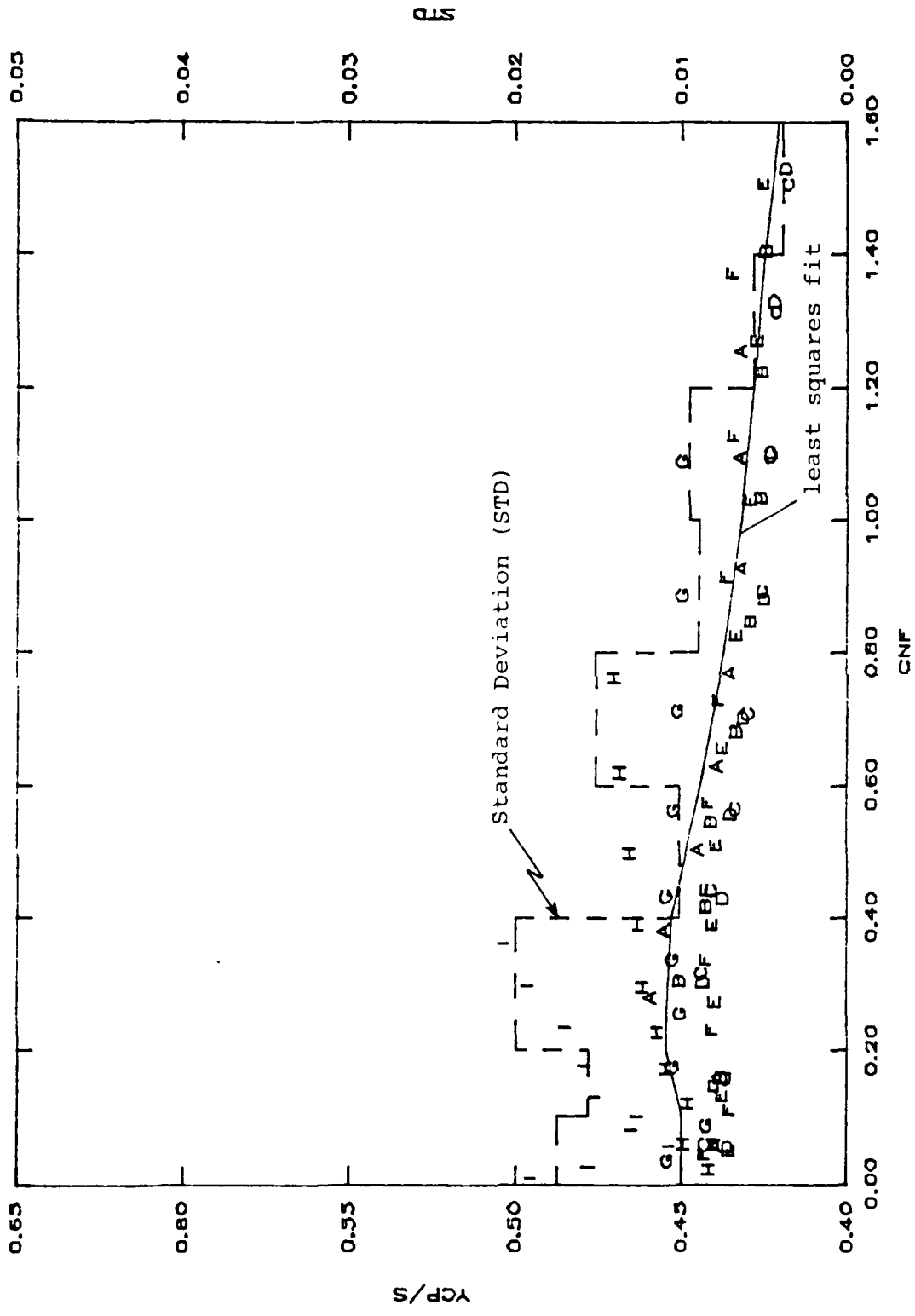


MACH = 2.5 AR = 1.00 TR = 0.5 D2 = 0 FIN 42

AVE. STD = 0.0075 GAMMA = 10.

(a) axial center-of-pressure location

Figure 13. Fin center-of-pressure correlation.



MACH = 2.5 AR = 1.00 TR = 0.5 D2 = 0 FIN 42

AVE. STD = 0.0139 GAMMA = 10.

(b) spanwise center-of-pressure location
Figure 13.- (Concluded).

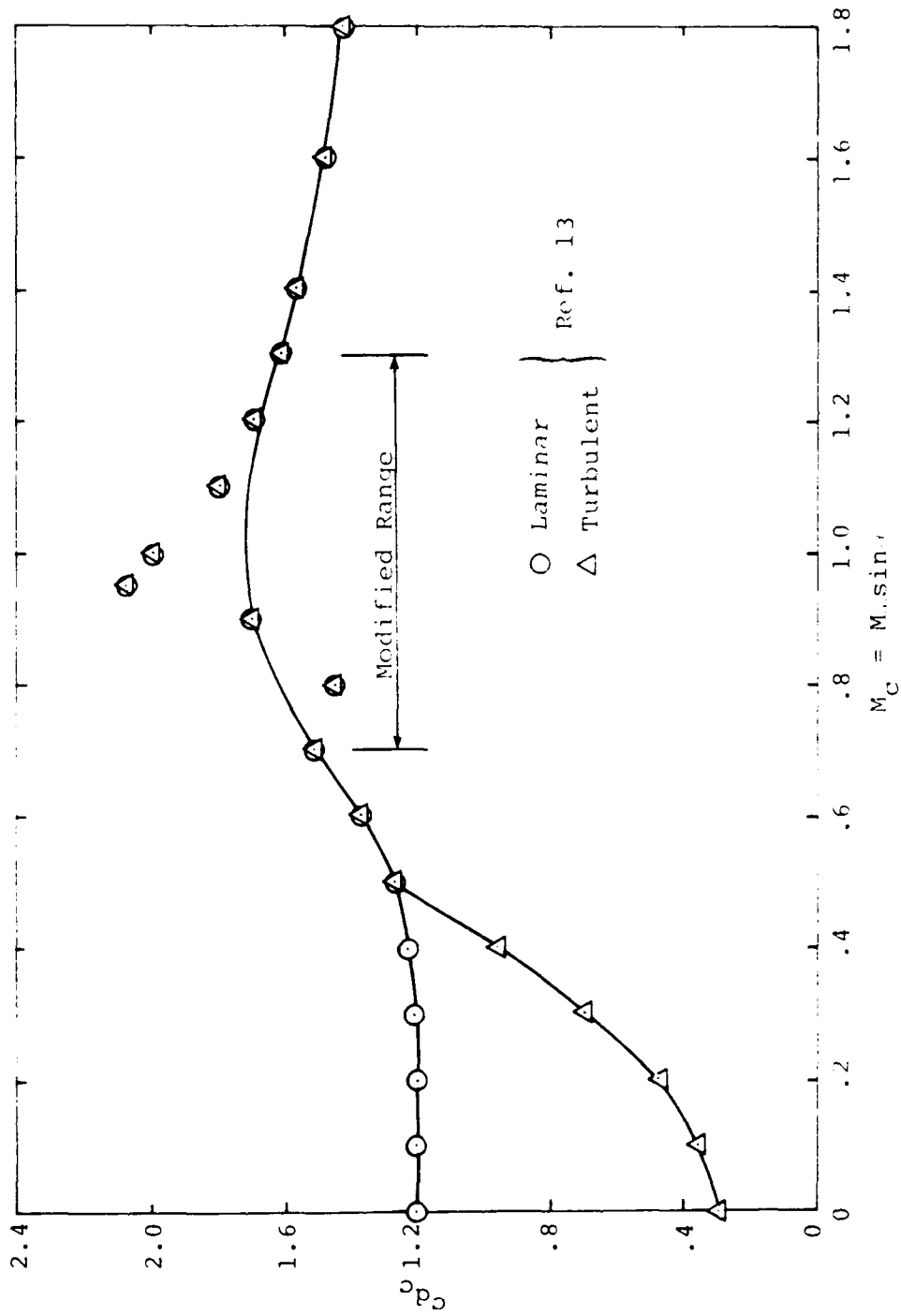
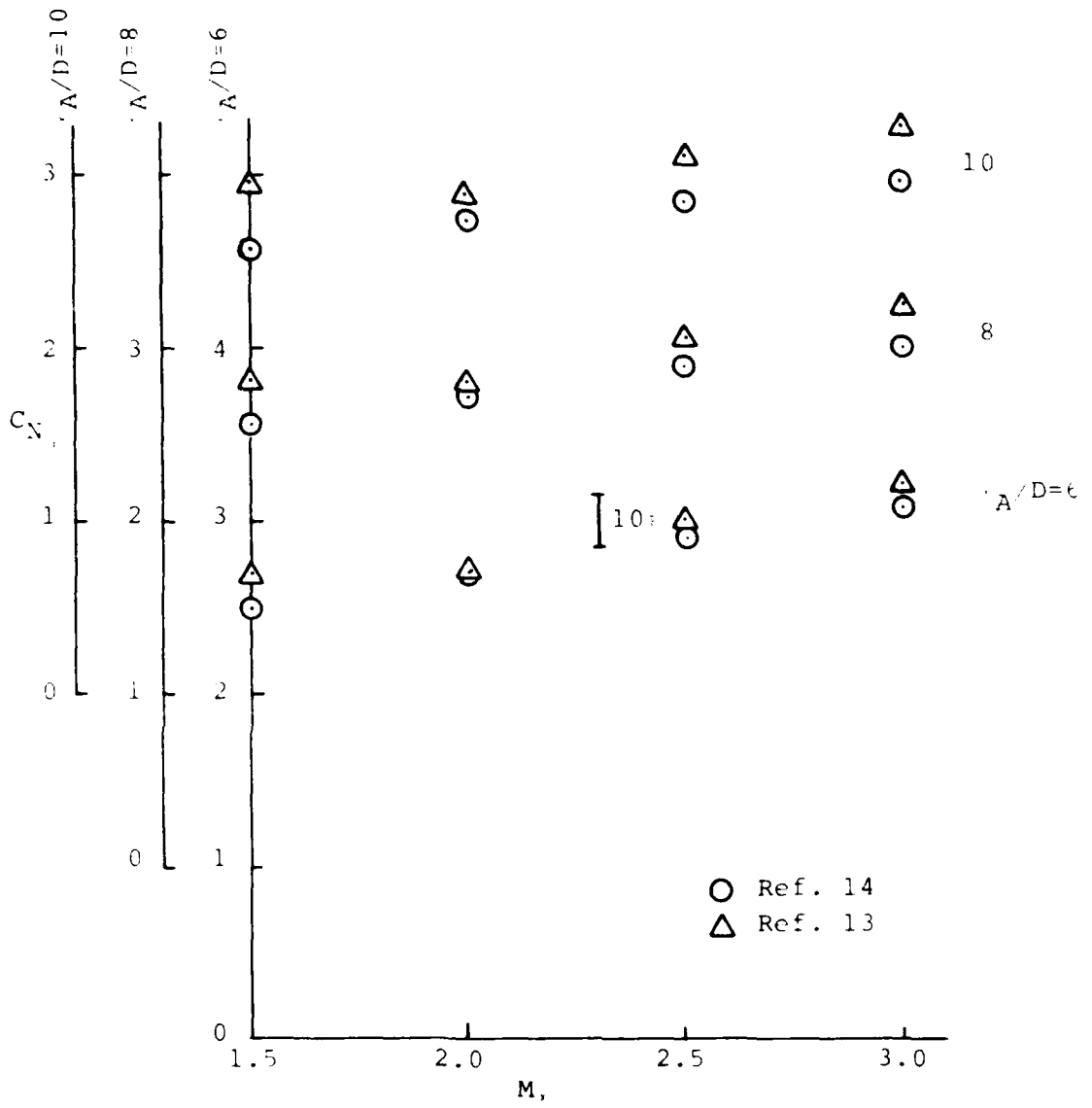
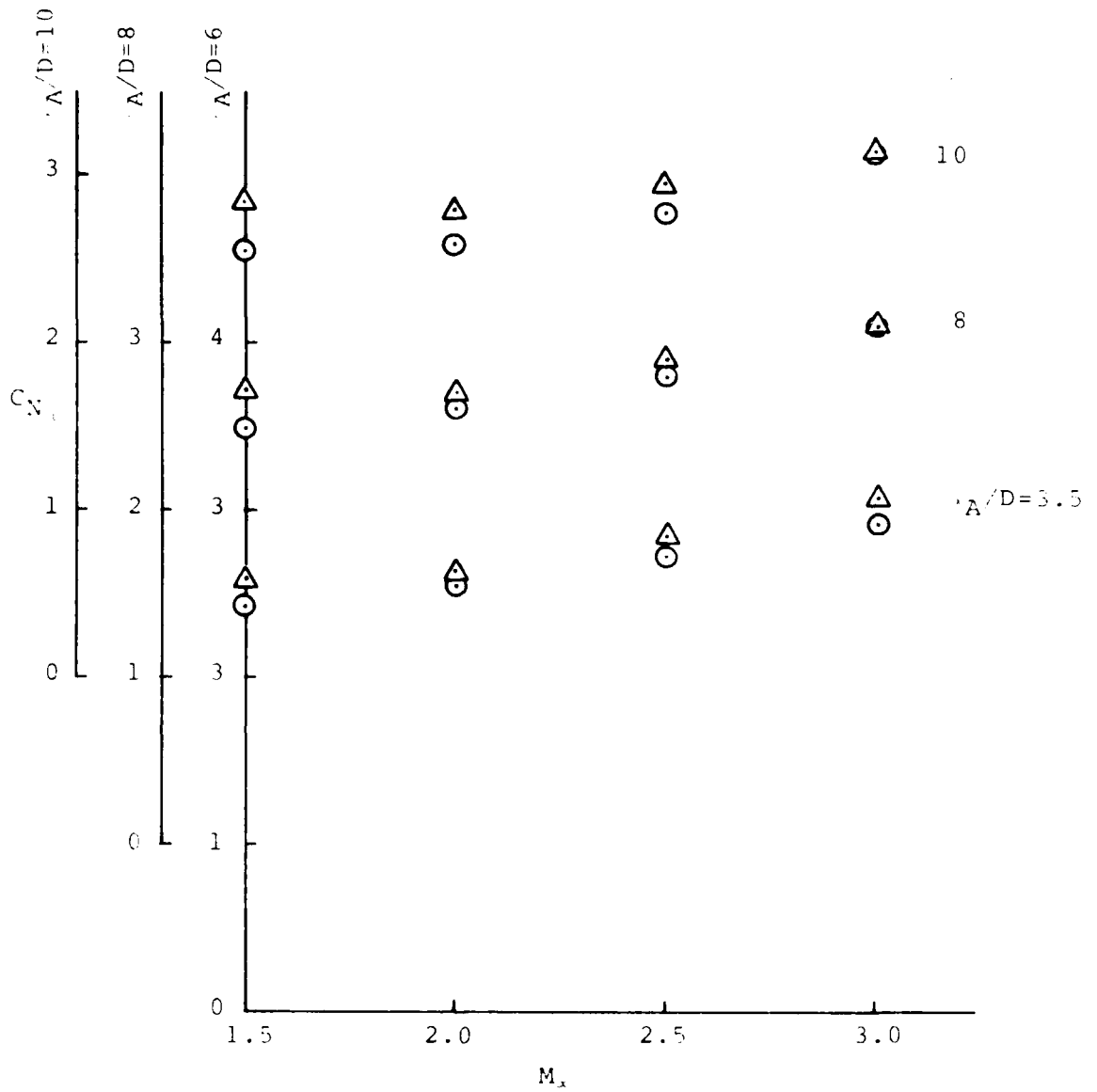


Figure 14.- Cross-flow drag coefficient.



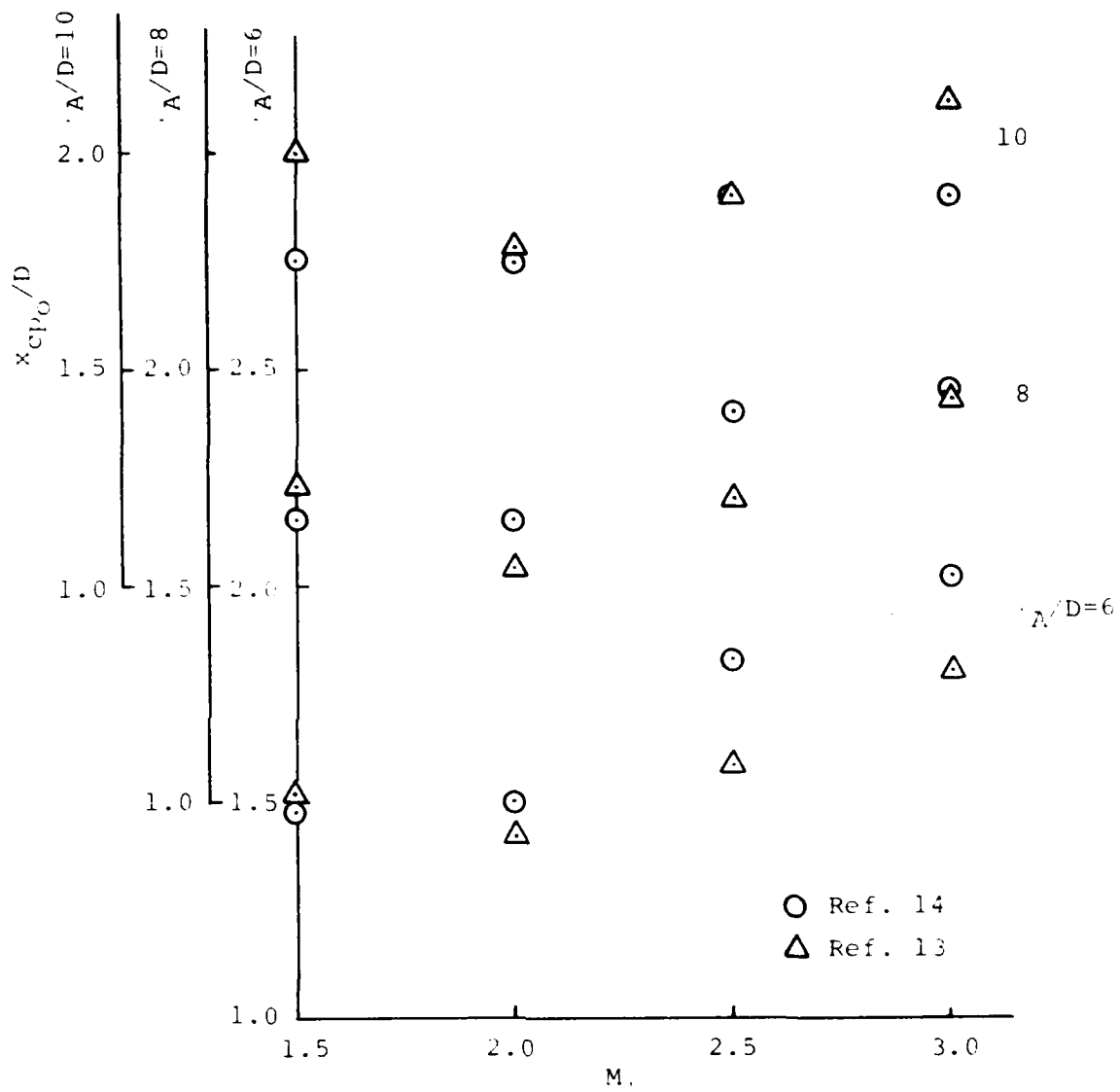
(a) $A/D = 2.5$

Figure 15.- Comparison of data bases for C_N



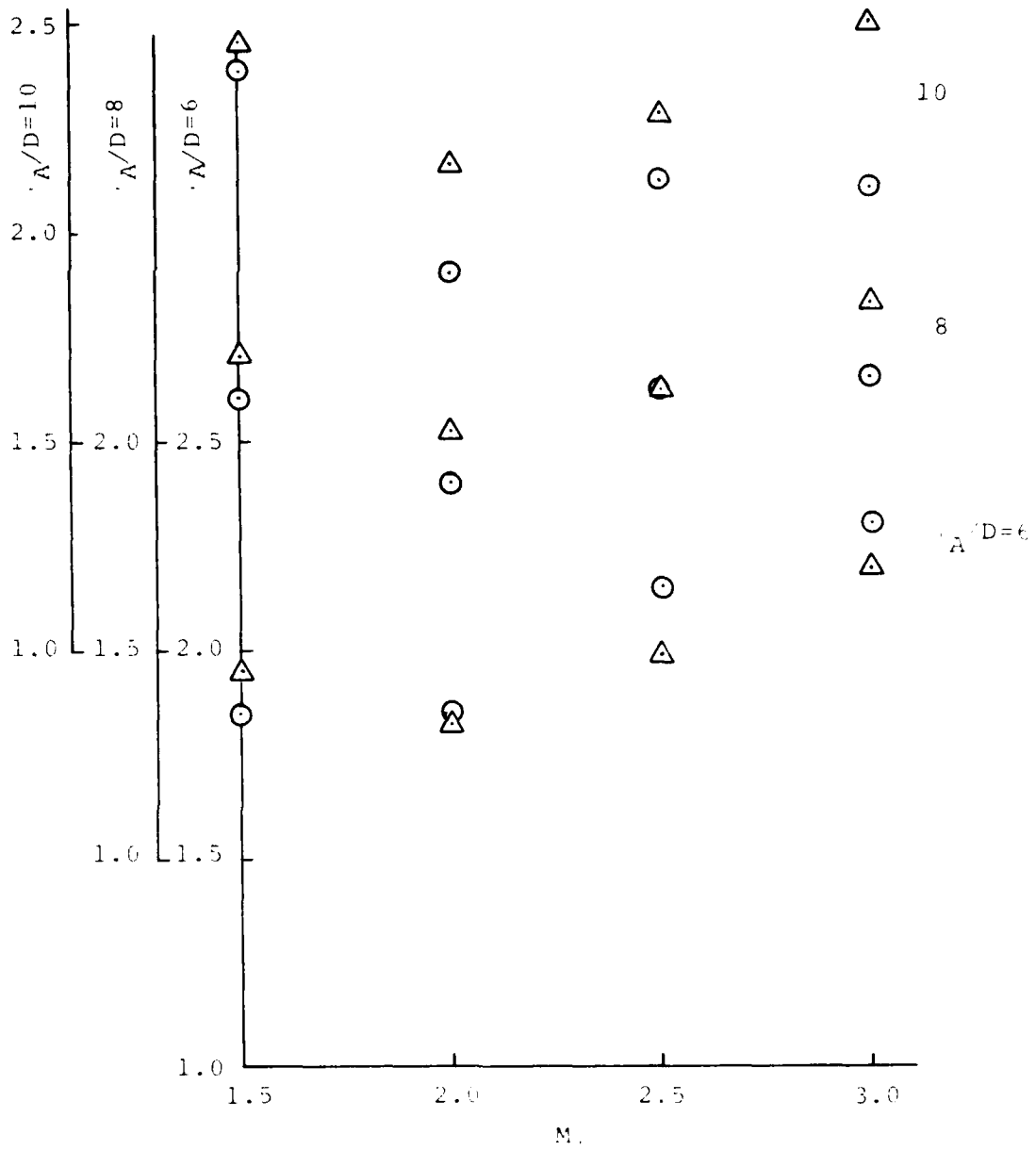
(b) $N/D = 3.5$

Figure 15.- Concluded.



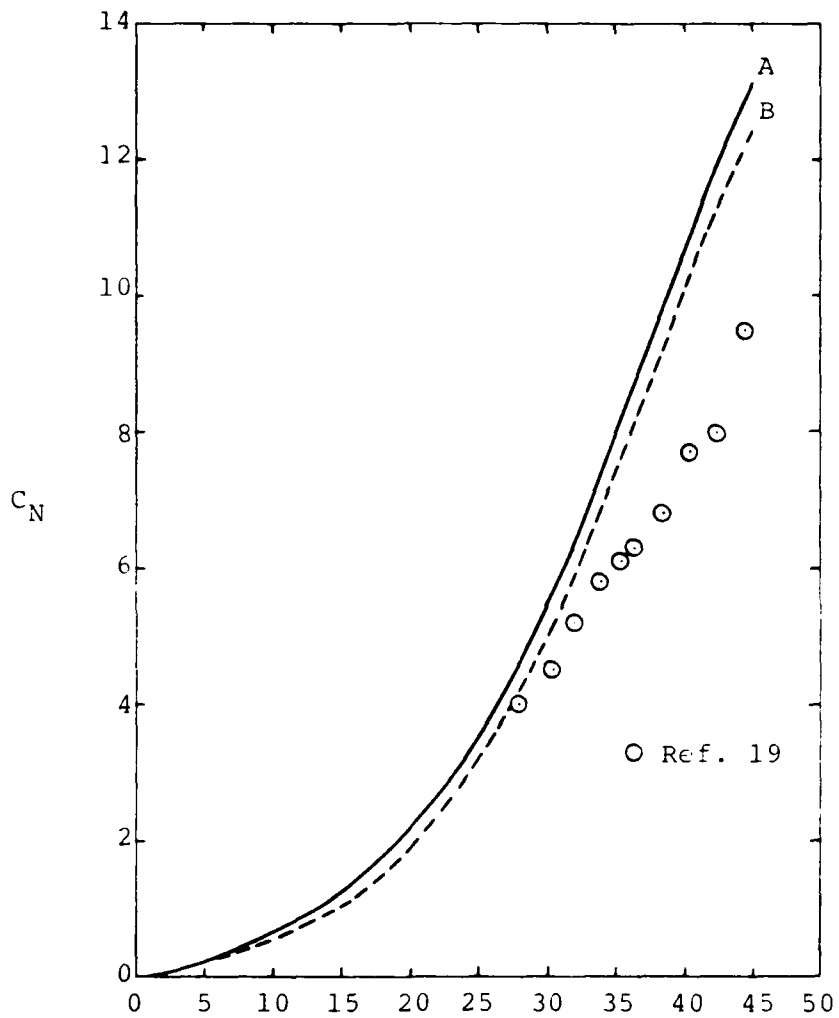
(a) $N/D = 2.5$

Figure 16.- Comparison of data bases for x_{cp0} .



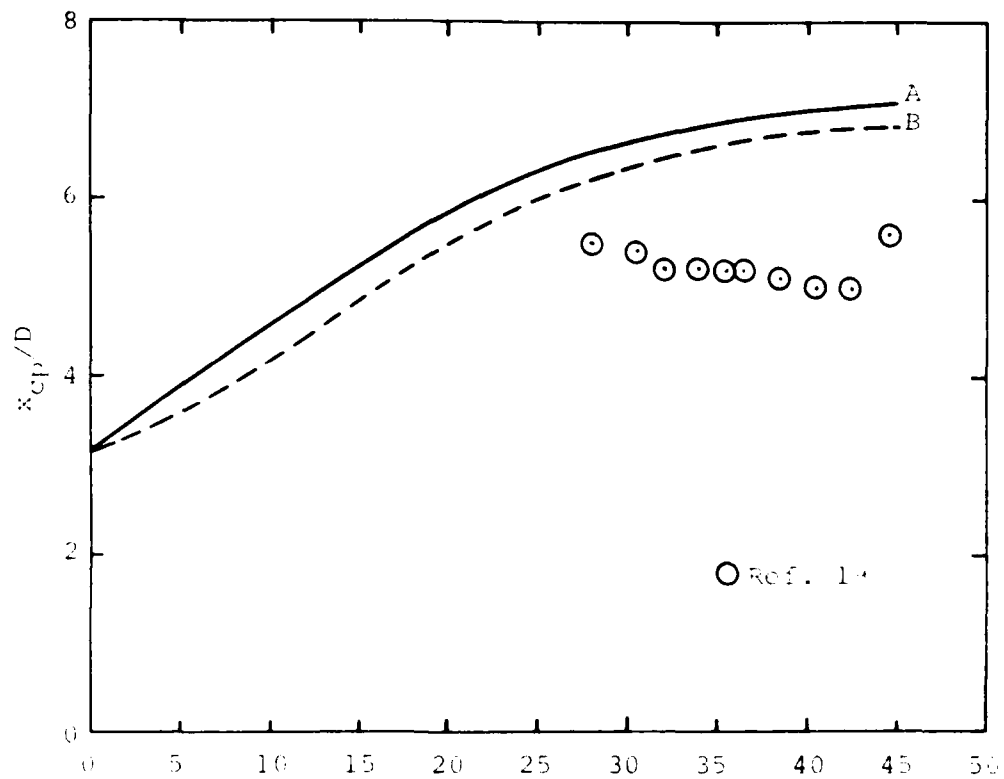
(b) $N/D = 3.5$

Figure 16.- Concluded.

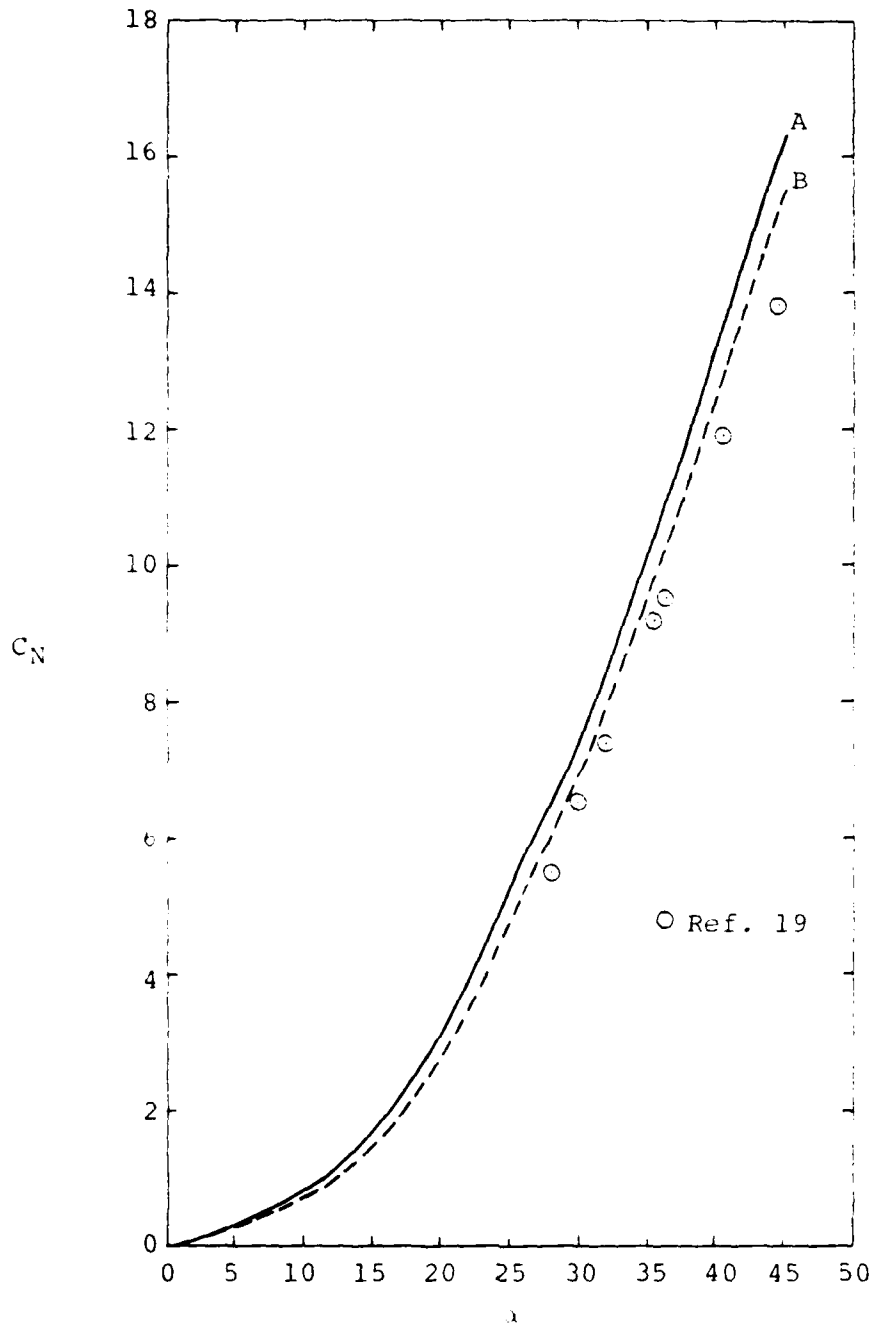


(a) C_N vs. α

Figure 17.- Comparison of predictions and data.
 $\delta_N/D = 1.5$, $\delta_A/D = 13$, $M_\alpha = 0.8$

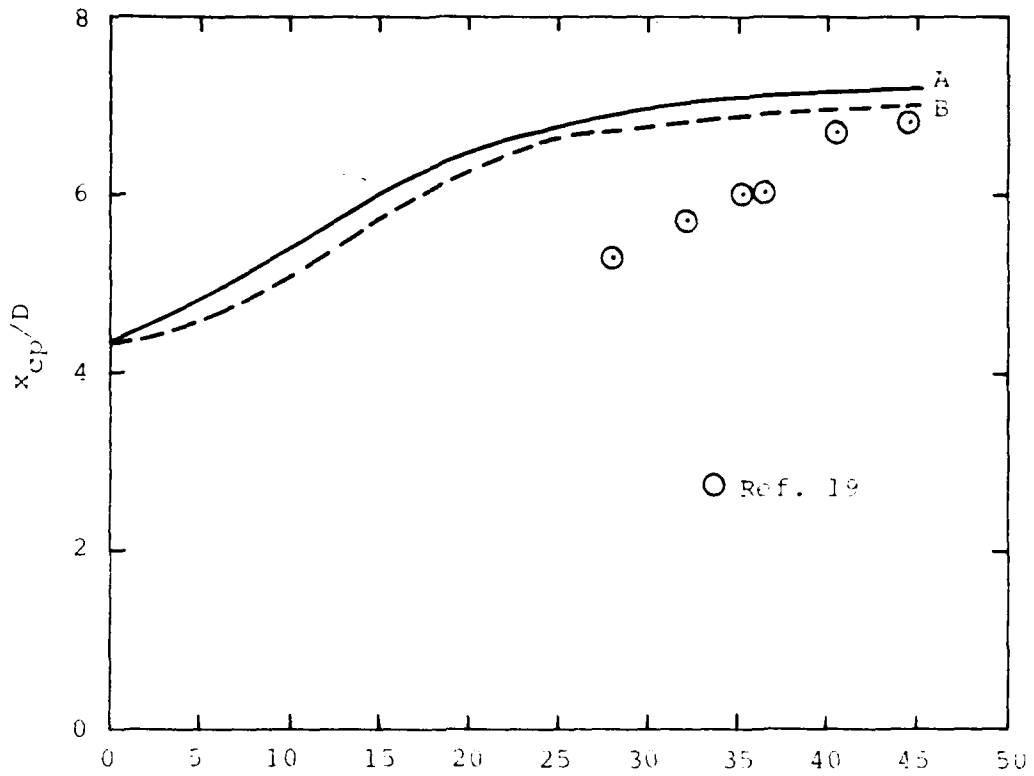


(b) x_{cp}/D vs.
Figure 17.- Concluded.

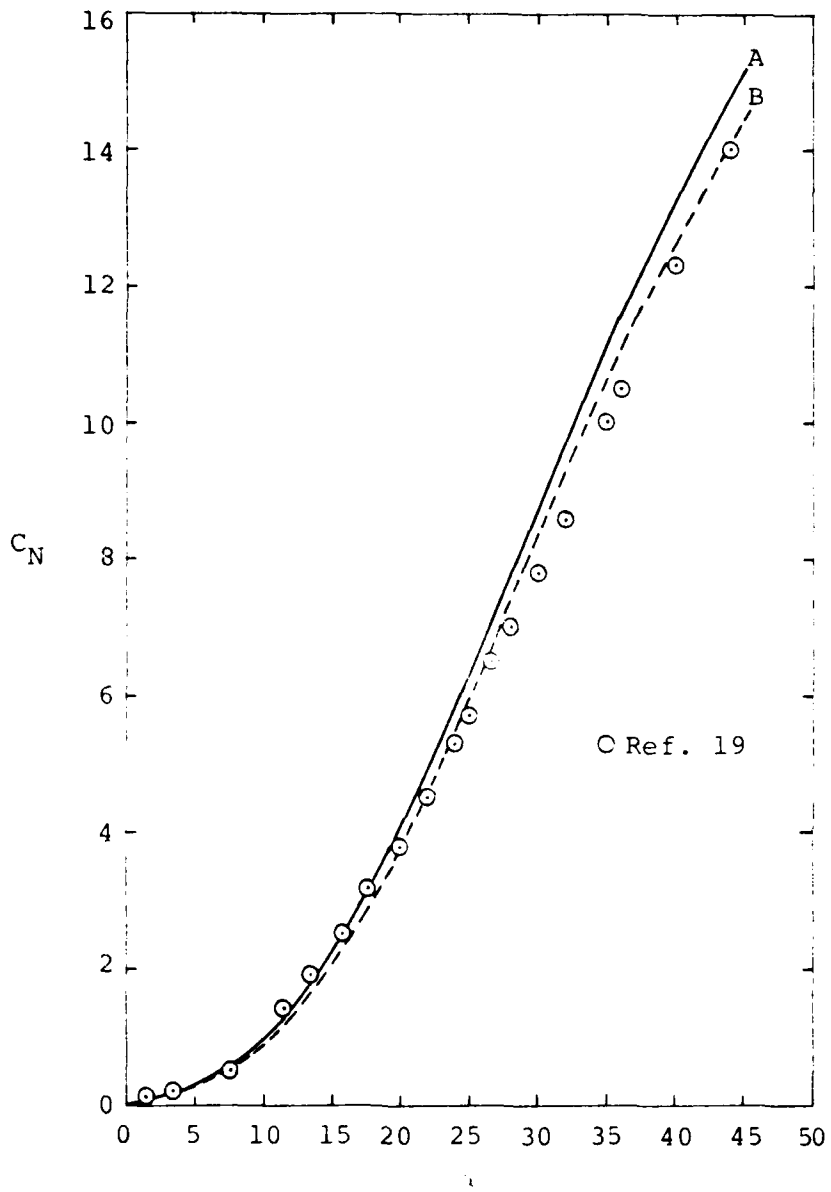


(a) C_N vs. λ

Figure 18.- Comparison of predictions and data.
 $\lambda_N/D = 1.5, \lambda_A/D = 13, M_\infty = 1.2$

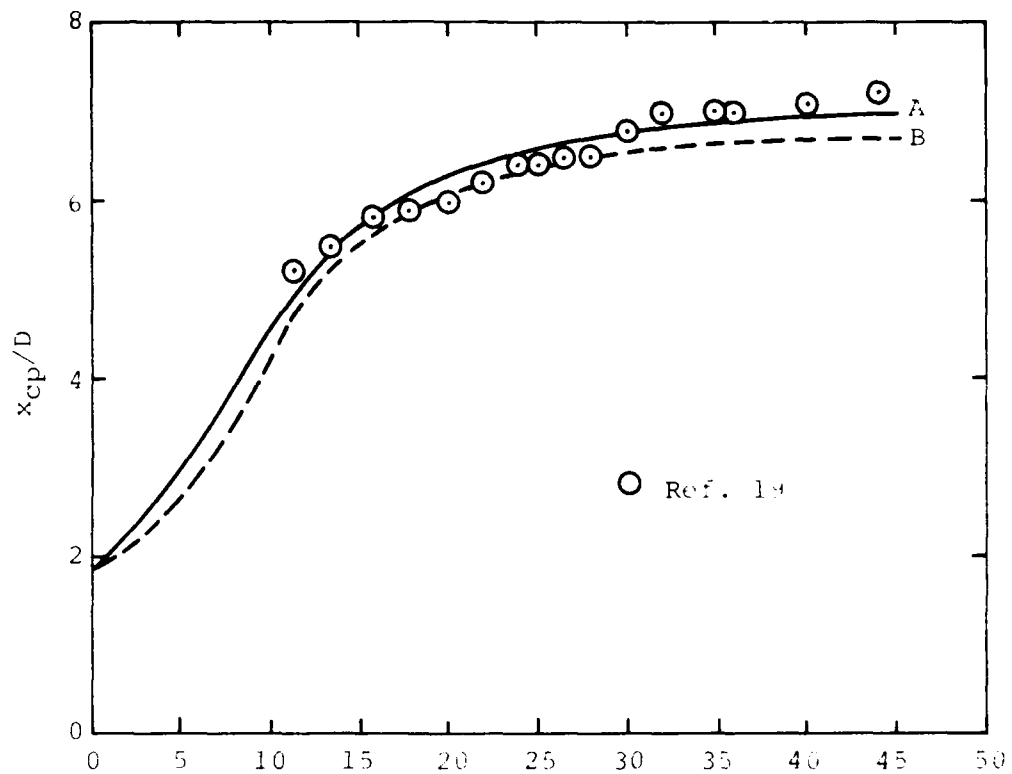


(L) x_{cp}/D vs.
Figure 18.- Concluded.



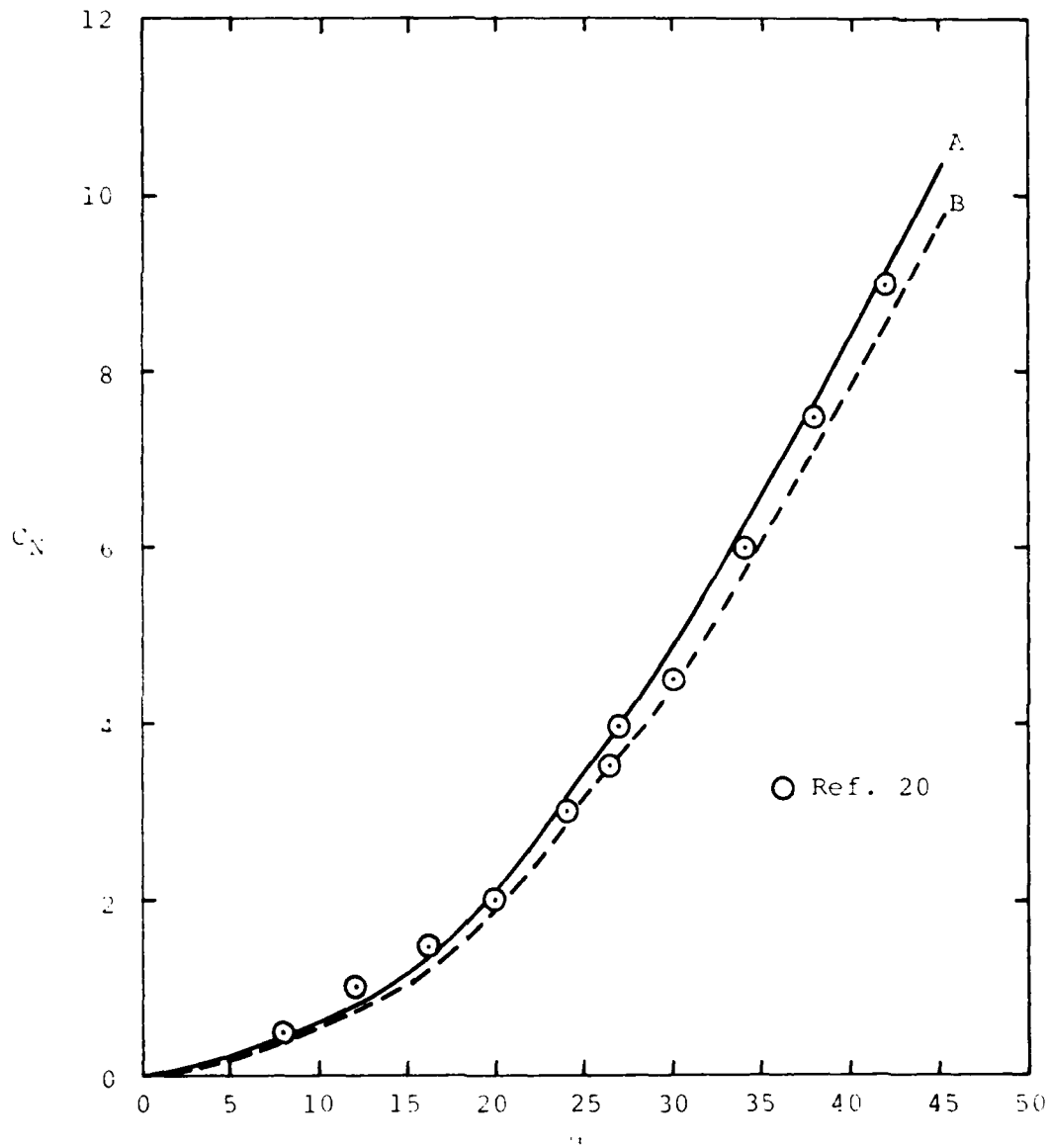
(a) C_N vs. α

Figure 19.- Comparison of predictions and data.
 $\beta_{N/D} = 1.5$, $\beta_{A/D} = 13$, $M_{\alpha} = 2.0$



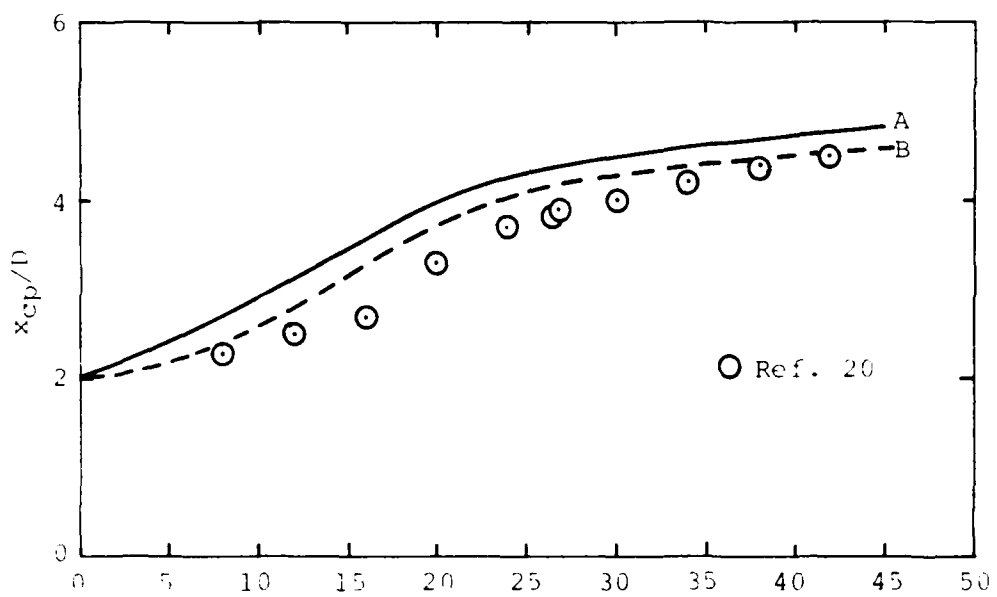
(b) x_{cp}/D vs.

Figure 19.- Concluded.

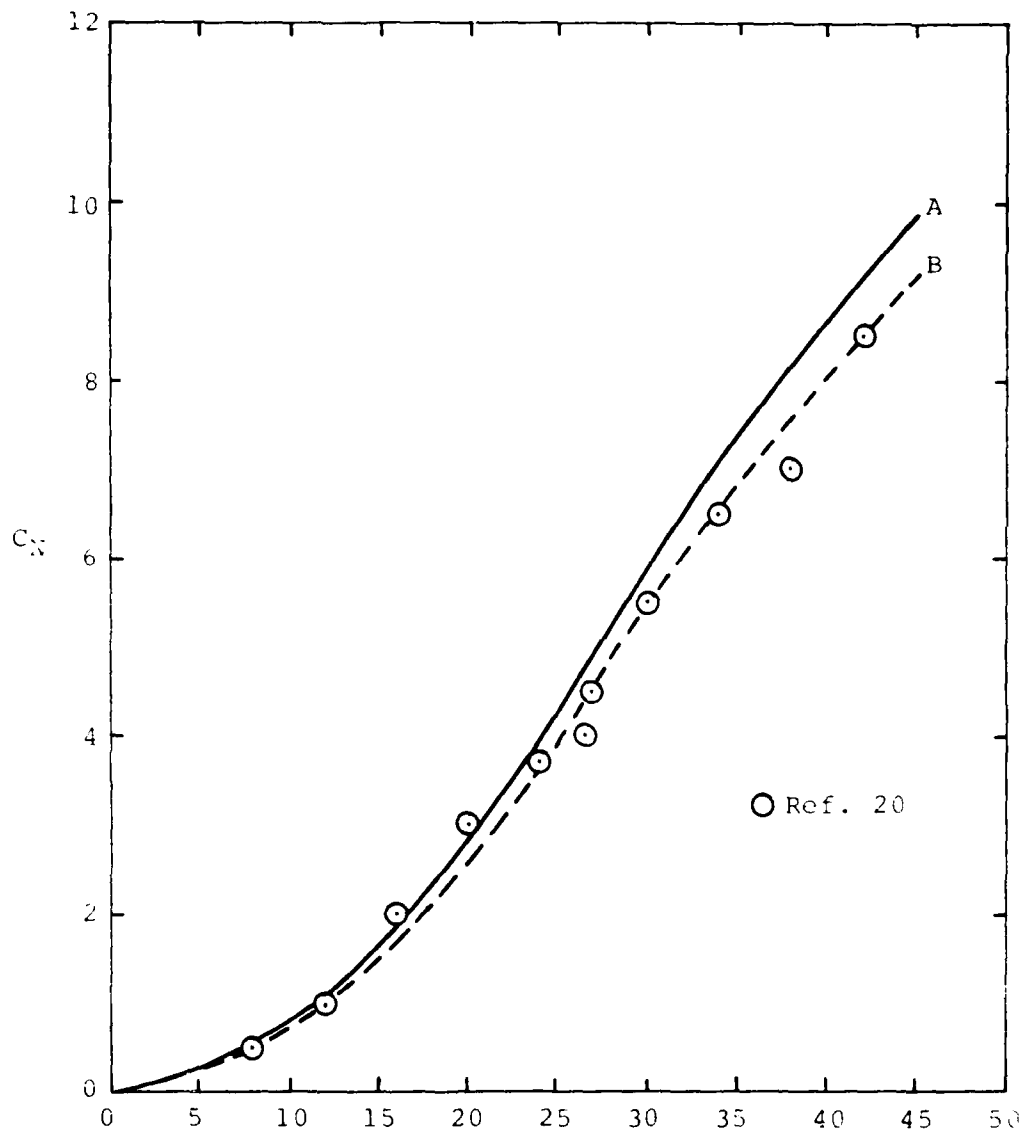


(a) C_N vs. x

Figure 20.- Comparison of predictions and data.
 $\sqrt{D} = 2.5$, $A/D = 7$, $M_0 = 1.2$

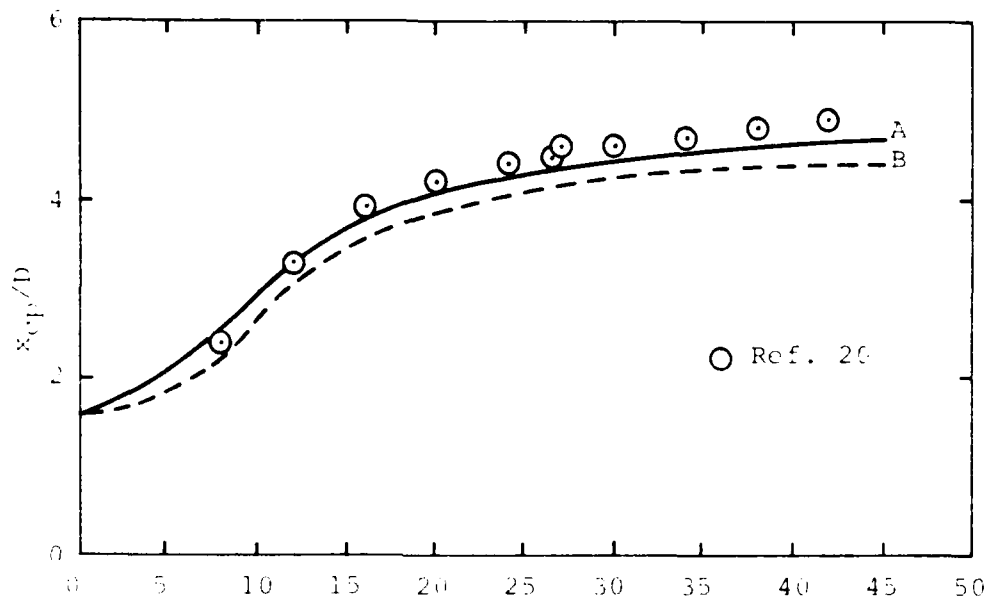


(b) x_{cp}/D vs. . . .
 Figure 20.- Concluded.



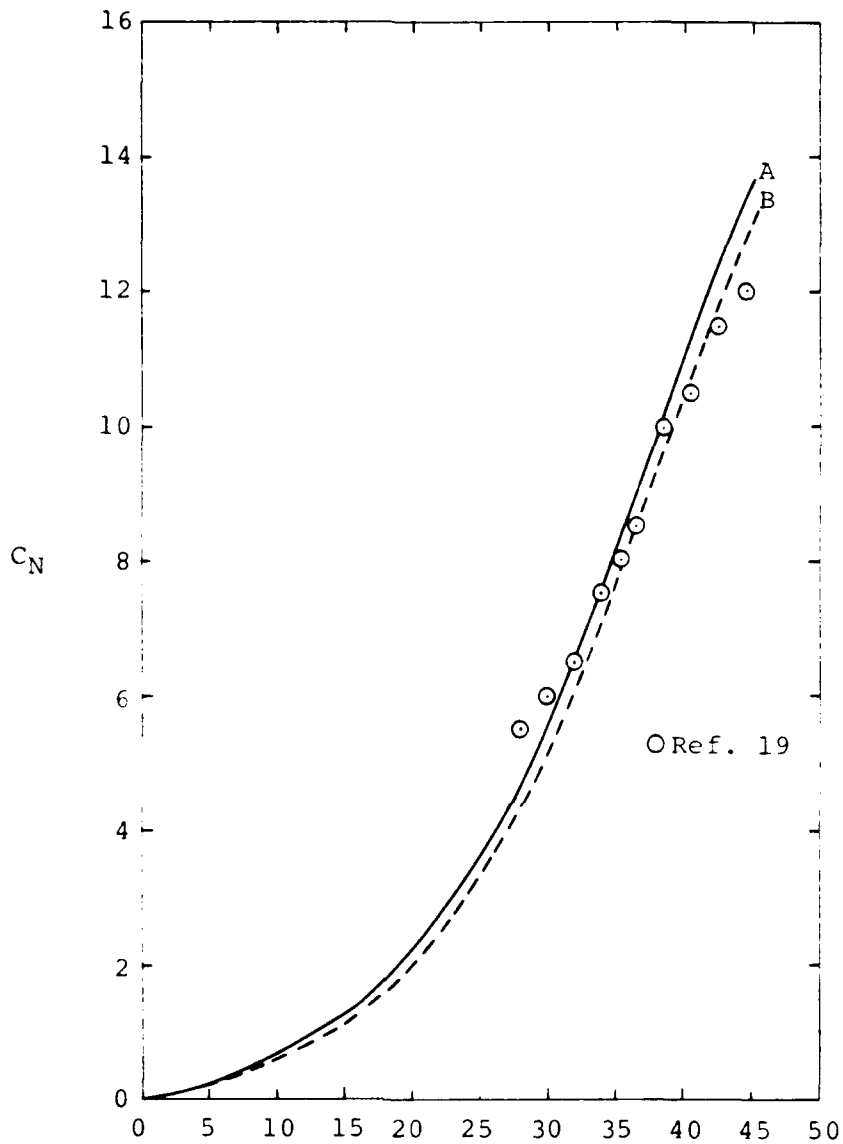
(a) C_N vs. x

Figure 21.- Comparison of predictions and data.
 $N/D = 2.5$, $A/D = 7$, $M_\infty = 2.0$



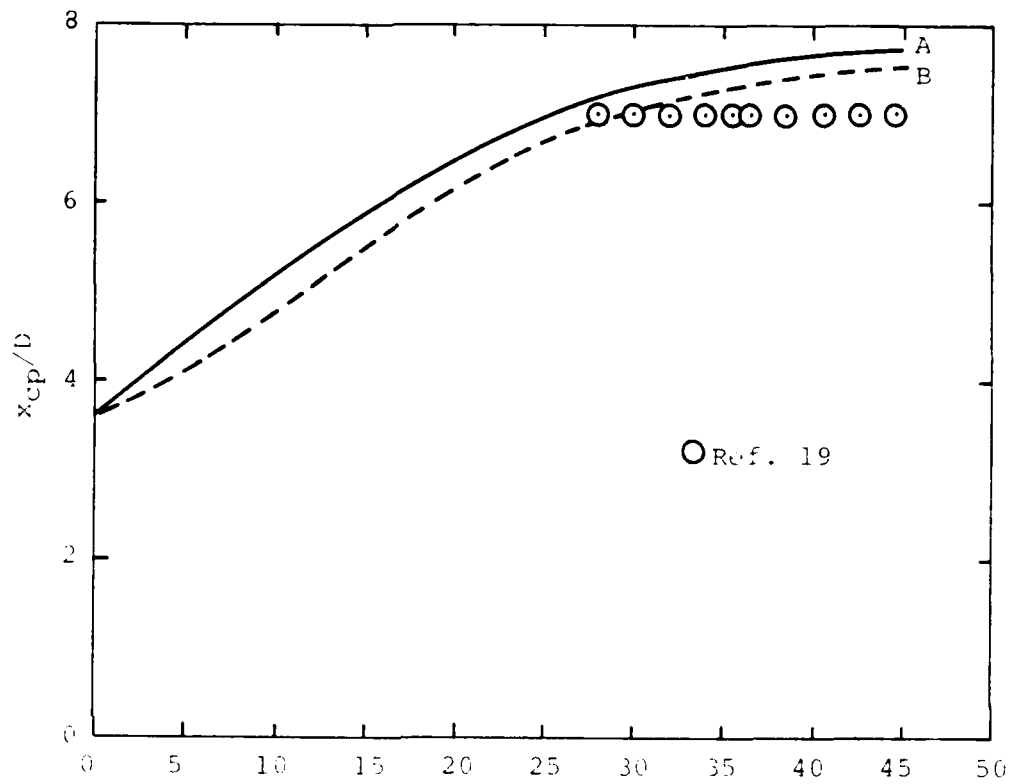
(b) x_{cp}/D vs.

Figure 21.- Concluded.

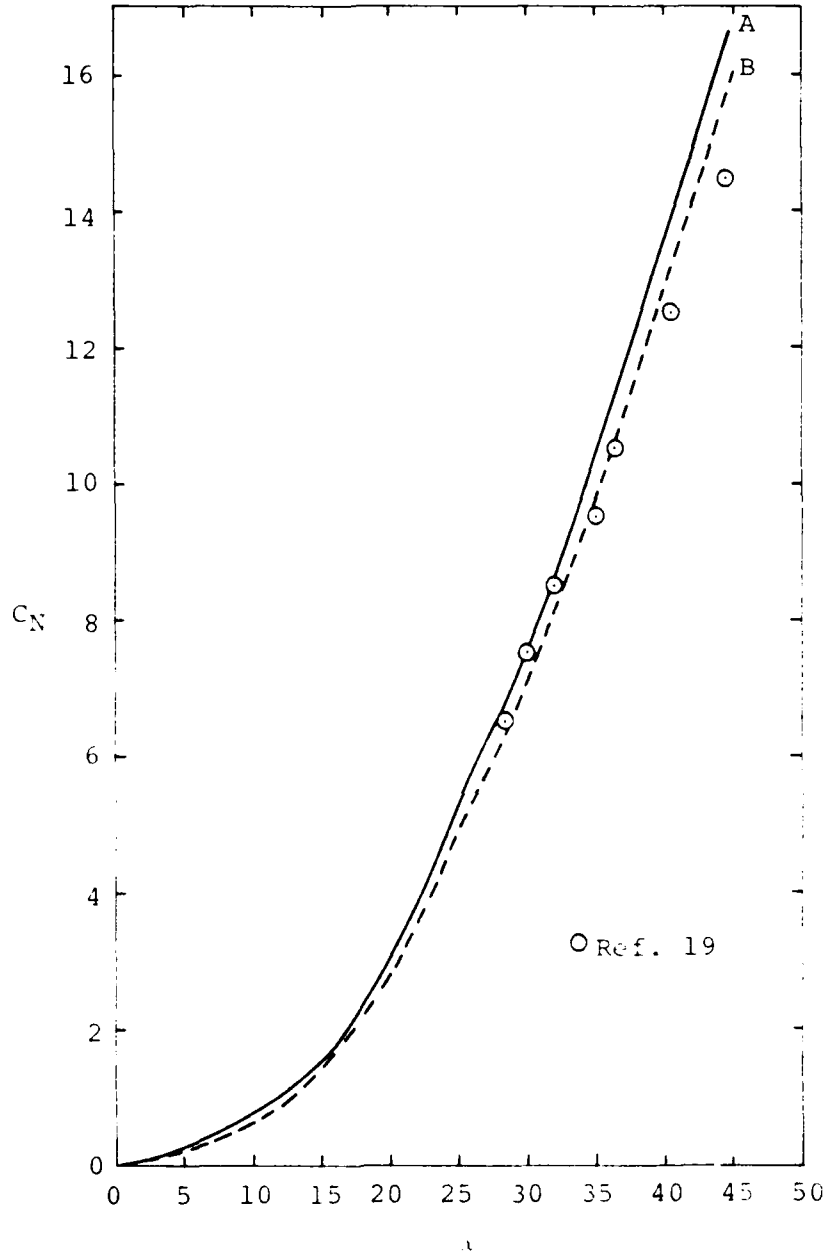


(a) C_N vs. α

Figure 22.- Comparison of predictions and data.
 $c_{N/D} = 2.5$, $c_{A/D} = 13$, $M_\infty = 0.8$

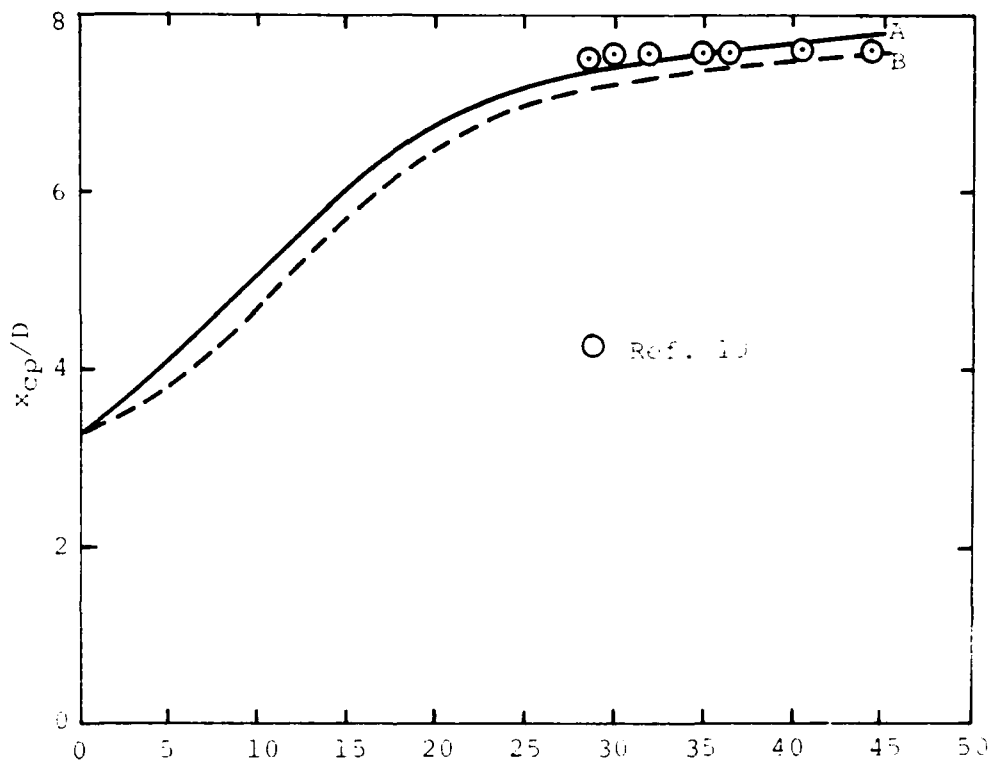


(b) x_{cp}/D vs. x
 Figure 22.- Concluded.



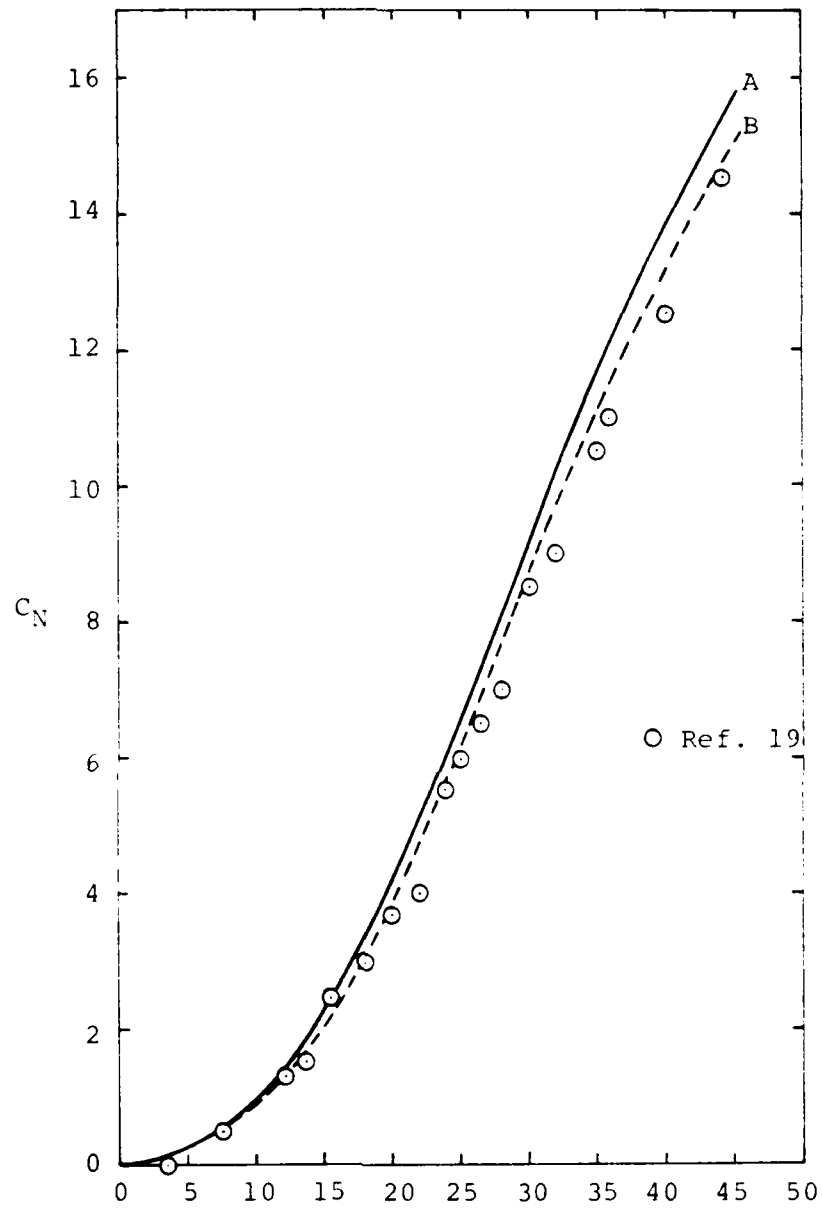
(a) C_N vs. α

Figure 23.- Comparison of predictions and data.
 $C_N/D = 2.5, \rho_A/D = 13, M_1 = 1.2$



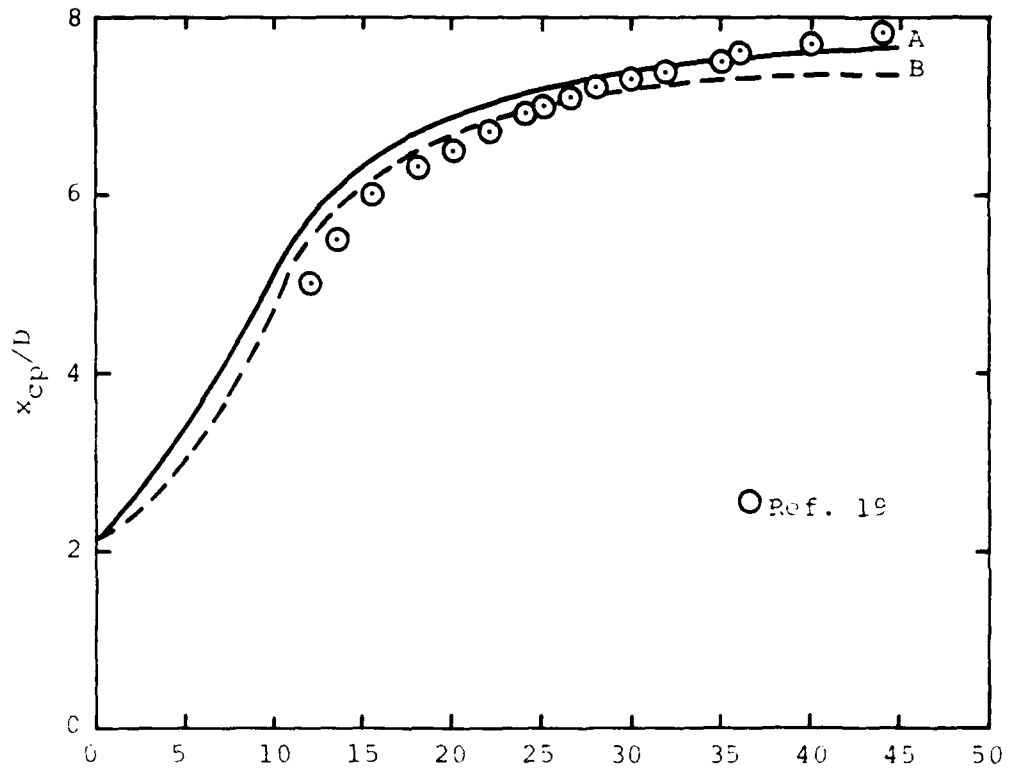
(b) x_{cp}/D vs. x

Figure 23. Concluded.



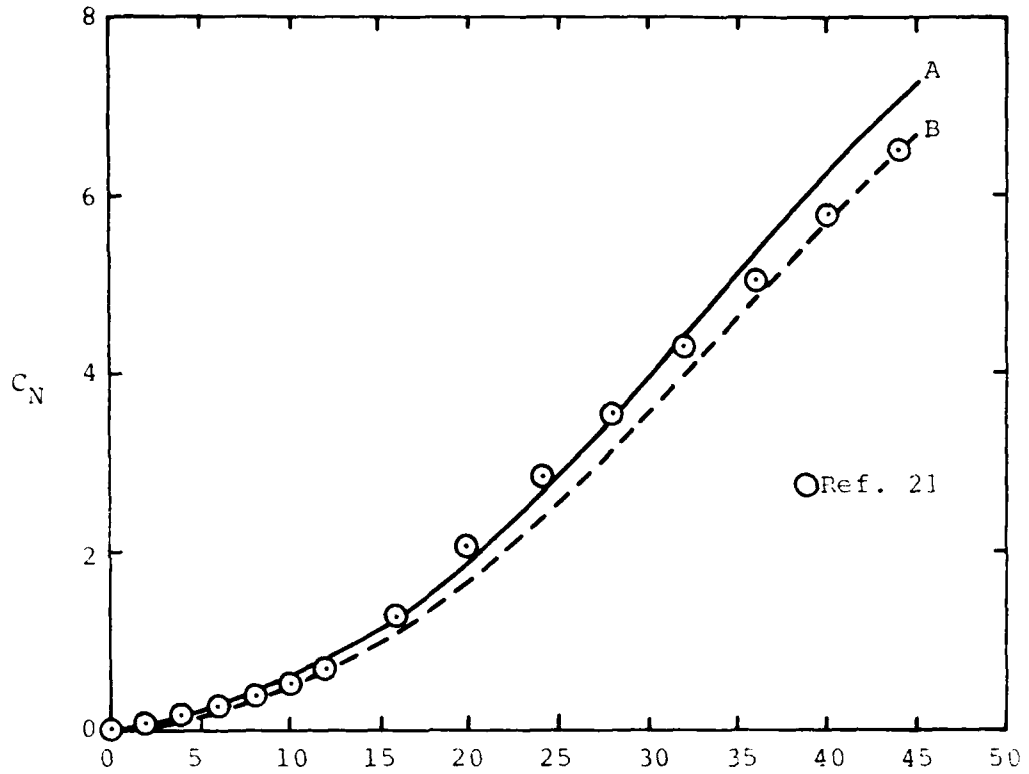
(a) C_N vs. α

Figure 24.- Comparison of predictions and data.
 $x_N/D = 2.5$, $x_A/D = 13$, $M_\infty = 2$

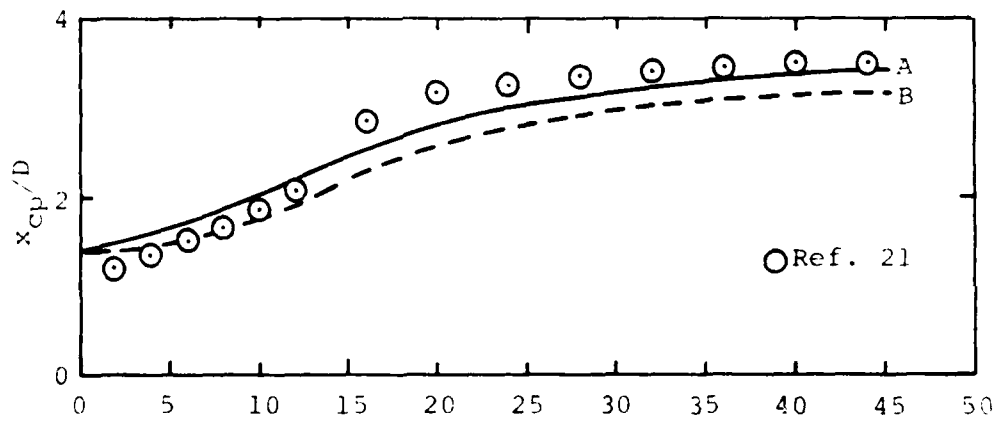


(b) x_{cp}/D vs. .

Figure 24.- Concluded.

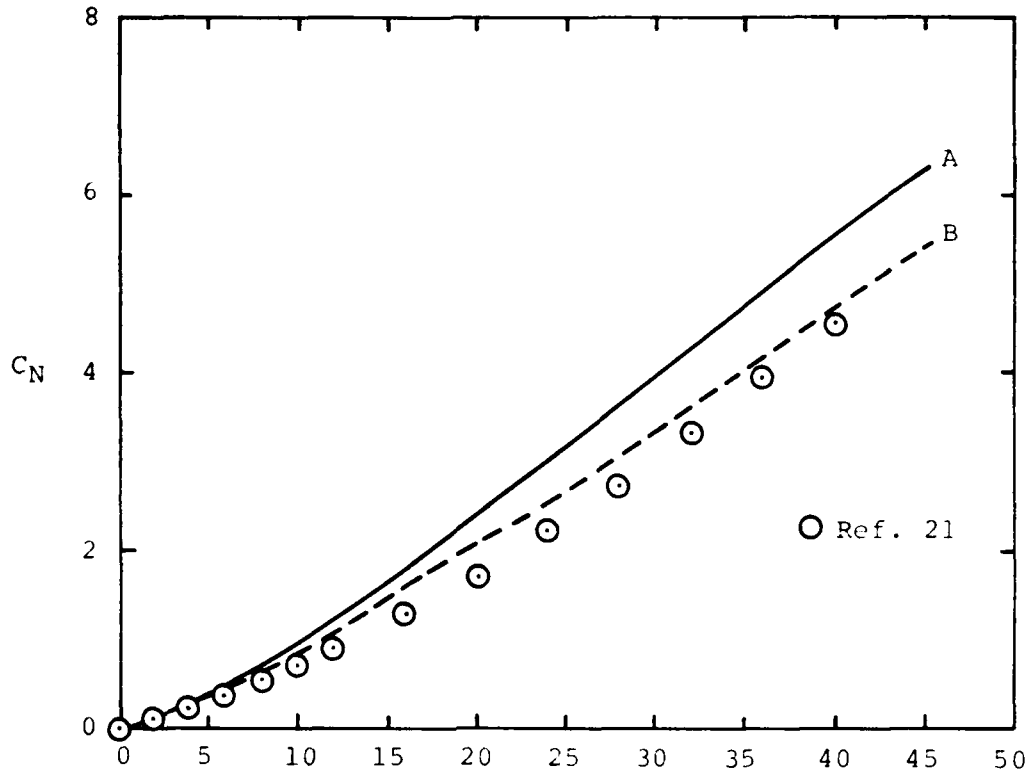


(a) C_N vs. x/D

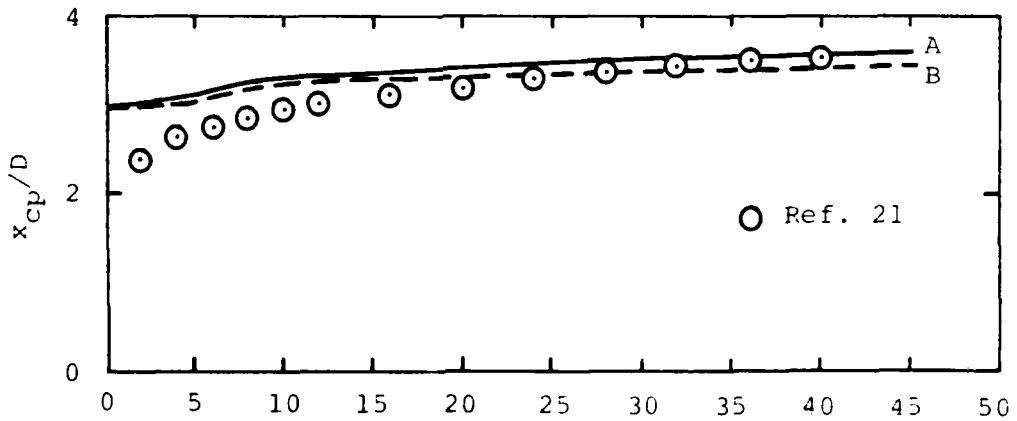


(b) x_{cp}/D vs. x/D

Figure 25.- Comparison of predictions and data.
 $\rho N/D = 3.0$, $\rho A/D = 3.667$, $M_\infty = 1.6$

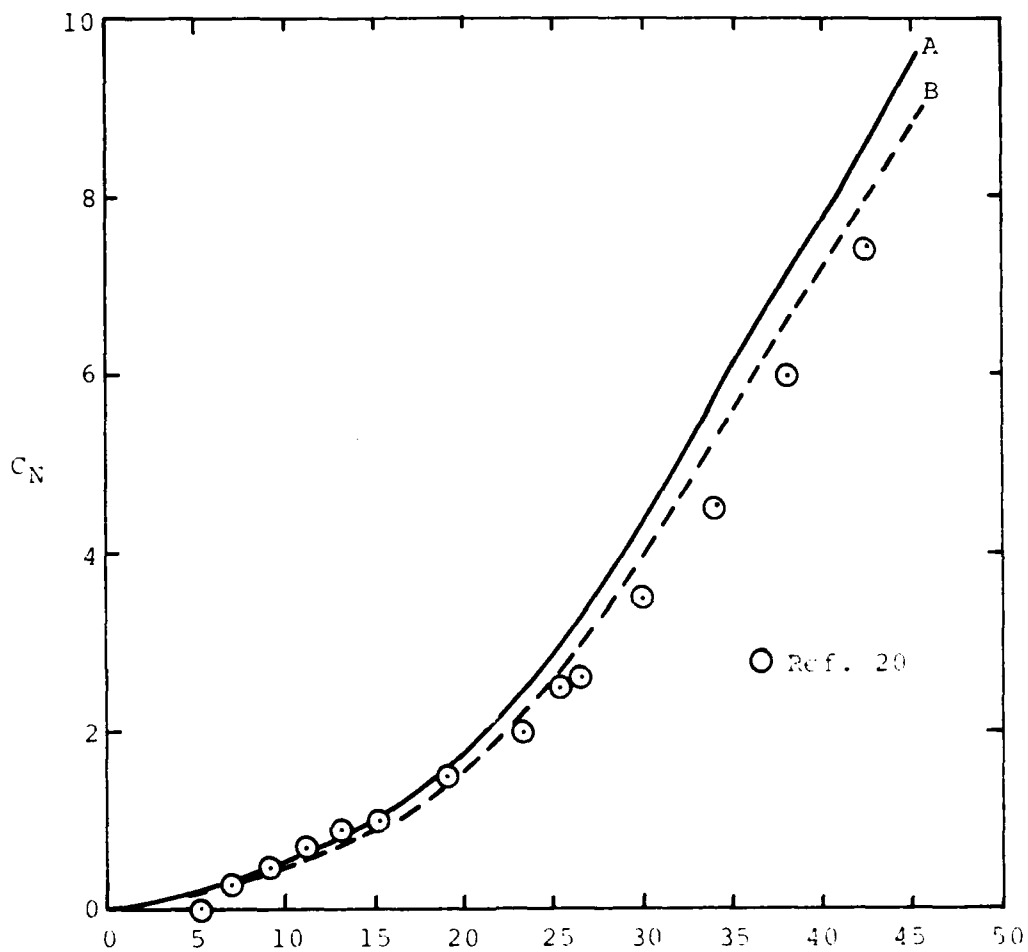


(a) C_N vs. x



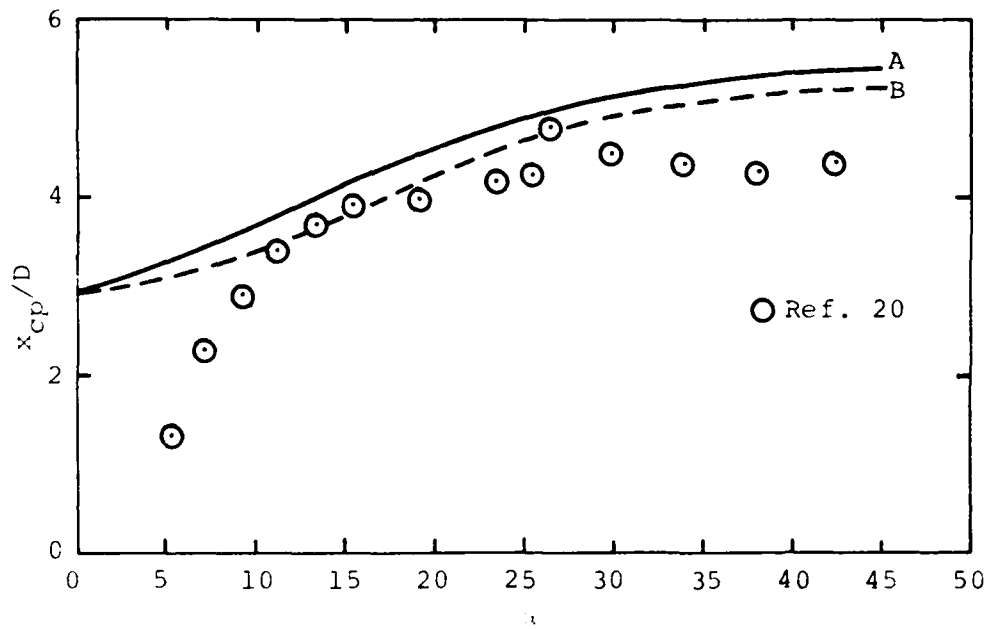
(b) x_{cp}/D vs. x

Figure 26.- Comparison of predictions and data.
 $\rho_N/D = 3.0$, $\rho_A/D = 3.667$, $M_\infty = 4.63$



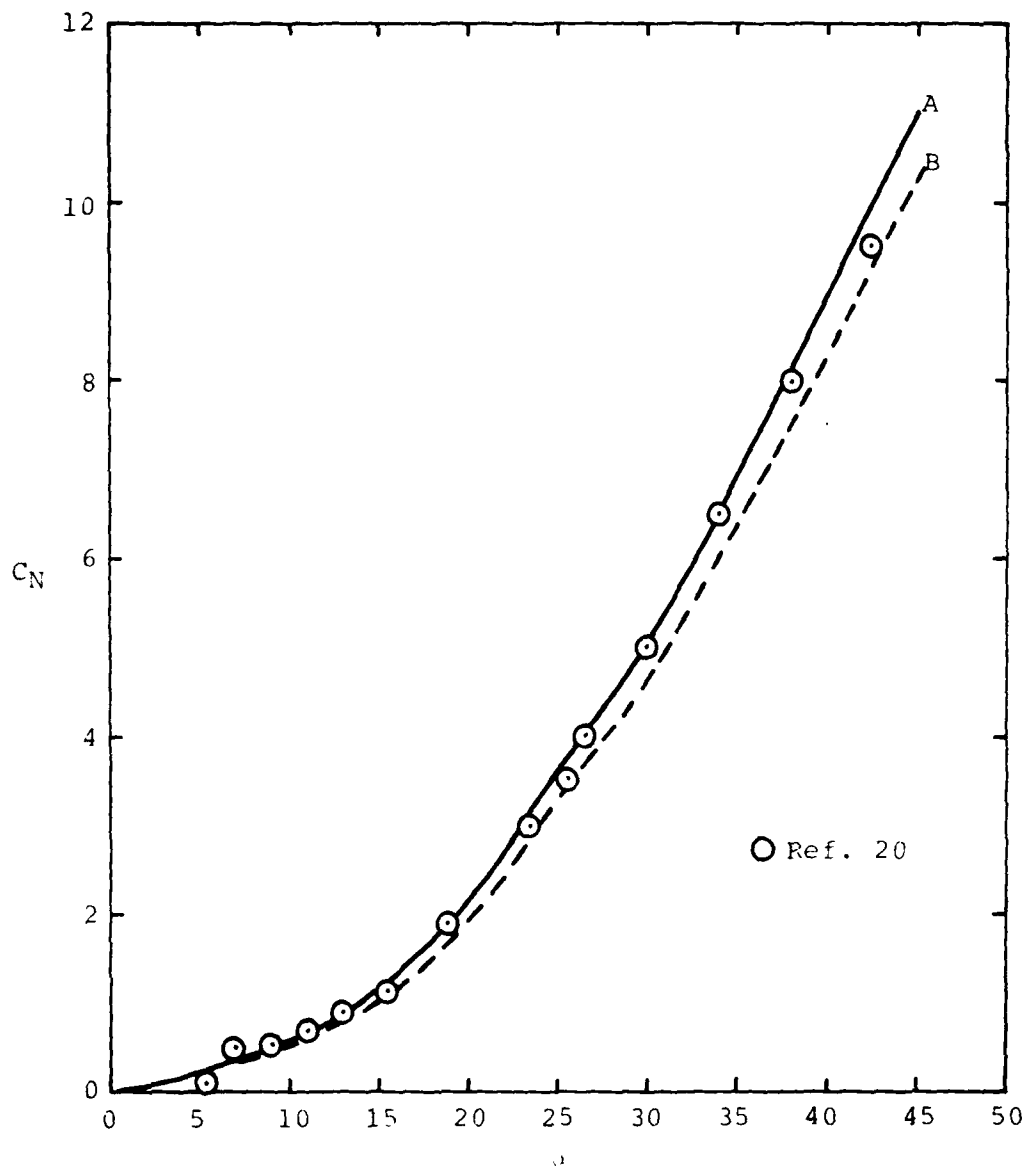
(a) C_N vs. x

Figure 27.- Comparison of predictions and data.
 $x_N/D = 3.5, x_A/D = 7, M_\infty = 0.9$



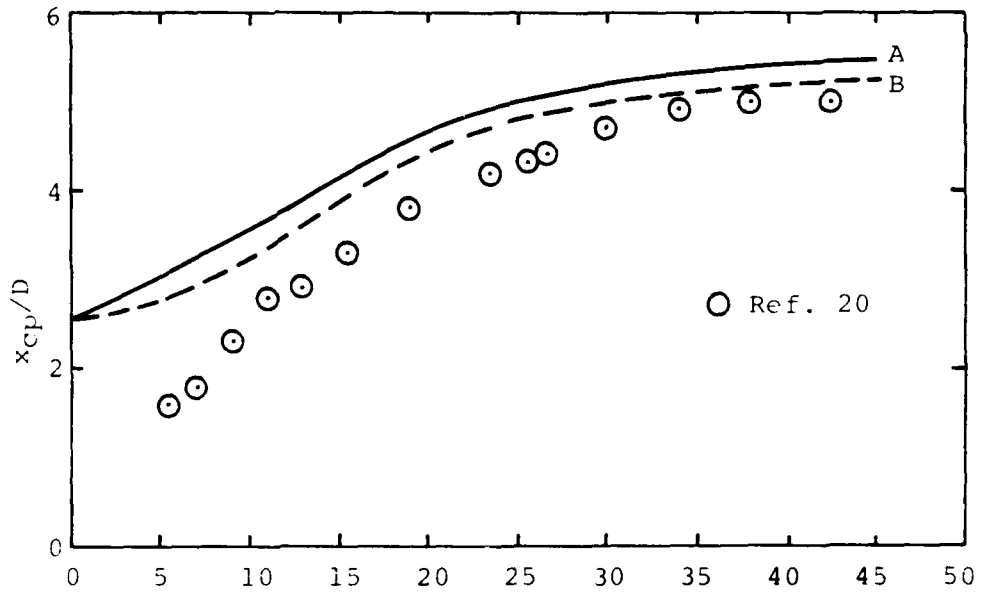
(b) x_{cp}/D vs. x

Figure 27.- Concluded.



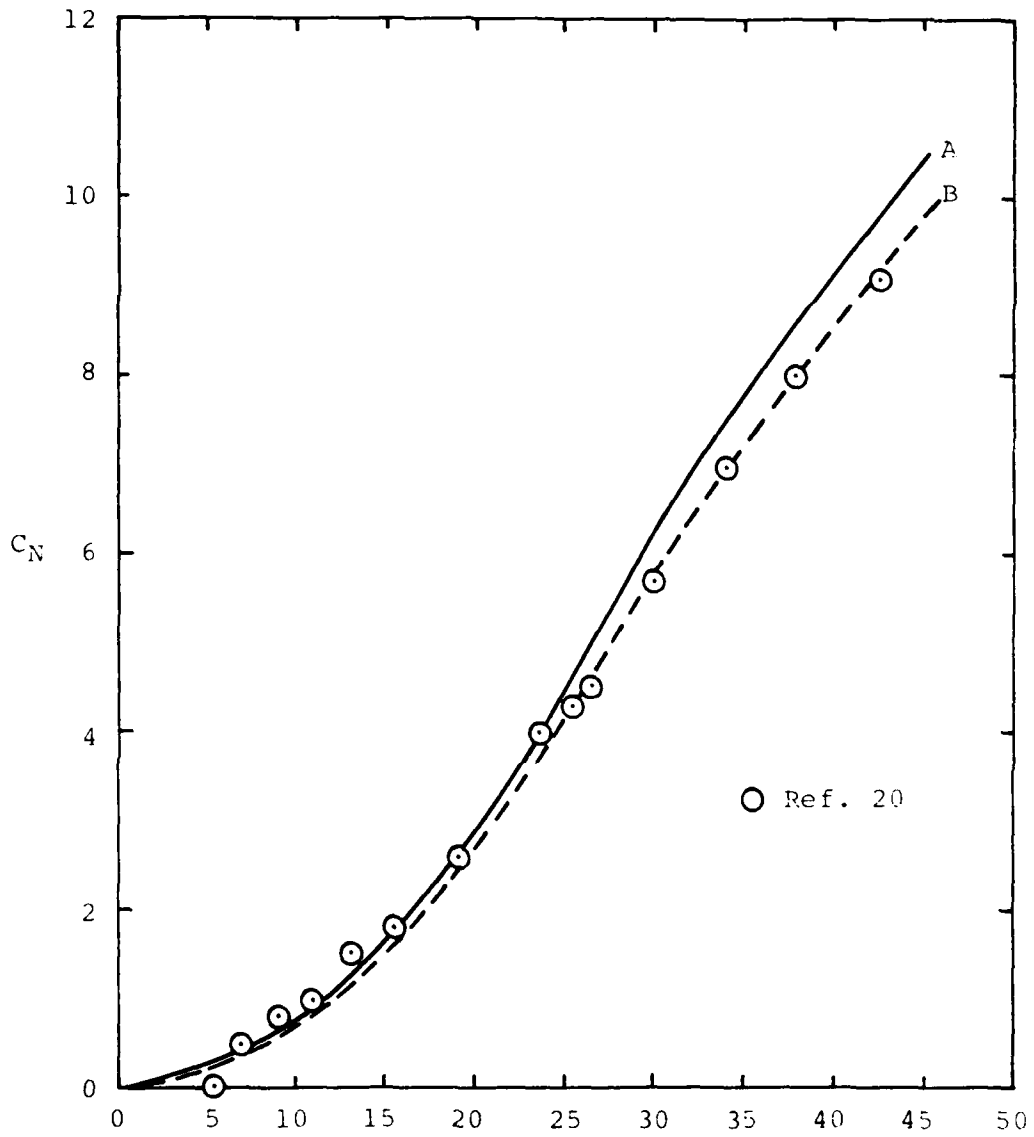
(a) C_N vs. x

Figure 28.- Comparison of predictions and data.
 $N/D = 3.5$, $A/D = 7$, $M_\infty = 1.2$



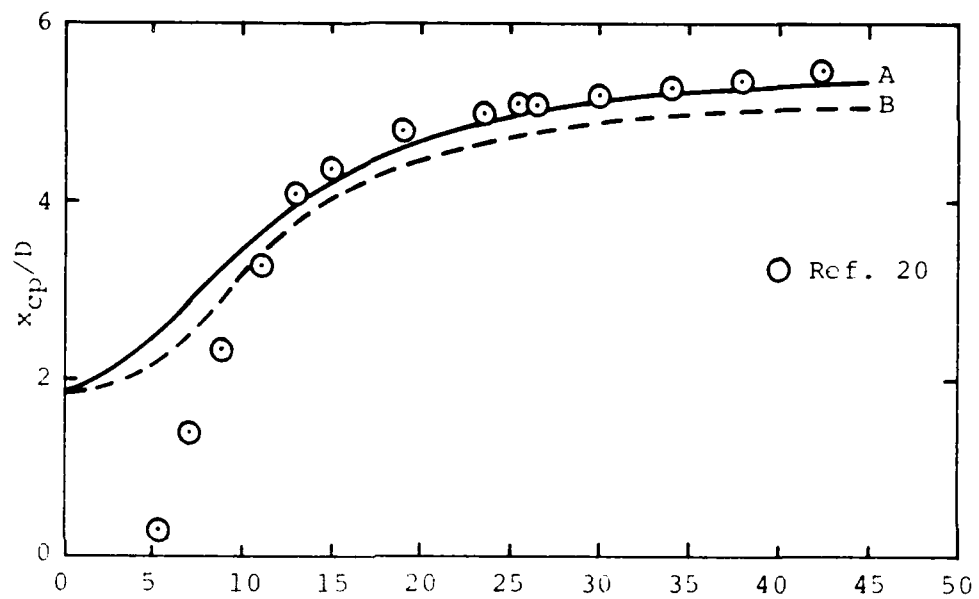
(b) x_{cp}/D vs. .

Figure 28.- Concluded.



(a) C_N vs. .

Figure 29.- Comparison of predictions and data.
 $N/D = 3.5, A/D = 7, M_\infty = 2.0$



(b) x_{cp}/D vs. α

Figure 29.- Concluded.

NOMENCLATURE

a	Body Radius
A_p	Planform area
AR	Aspect ratio of wing alone
A_{ref}	Reference area
c_{d_c}	Cross flow drag coefficient
c_r	Fin root chord
C_N	Normal-force coefficient
$C_{NF(B)_i}$	Normal-force coefficient of fin i in the presence of a circular body
C_{NSB}	Linear portion of the normal force acting on a body
C_{NV}	Nonlinear portion of the normal force acting on a body
C_{NW}	Normal-force coefficient of wing alone
$C_{N\alpha}$	Derivative of the normal-force coefficient with respect to α
D	Diameter of the cylindrical portion of a body
l_A	Length of the cylindrical portion of a body
l_N	Nose length
M_c	Cross flow Mach number
M_ℓ	Mach number at a point in a body-alone flow field
\bar{M}_ℓ	Local Mach number in presence of body alone averaged over exposed span of fin (equation (2))
M_∞	Free-stream Mach number
N	Normal force acting on the body
q_ℓ	Dynamic pressure at a point in a body-alone flow field
\bar{q}_ℓ	Local dynamic pressure in presence of body alone averaged over exposed span of fin (equation (1))
q_∞	Dynamic pressure of the free stream
r	Radial distance from body axis
r_a	Radius of curvature of tangent-ogive nose
s	Exposed semispan of a fin
s_m	Semispan of fin
V_∞	Free-stream velocity

NOMENCLATURE (CONTINUED)

x	Distance aft of nosetip
x_c	Axial location of the centroid of the planform area of a body
x_{cp}	Axial location of the center of pressure
x_{cp0}	Axial location of the center of pressure for the linear portion of the normal force
y_{cp}	Lateral location of the center of pressure of a fin
α	Angle of attack
α_c	Angle between body axis and wind velocity vector
α_{eqi}	Equivalent angle of attack of fin i ; i.e., angle of attack of wing alone which gives same normal-force coefficient as that of fin i
$\hat{\alpha}_{eqi}$	Equivalent angle of attack of fin i if all fins are undeflected
δ_i	Deflection of fin i , positive when the leading edge is rotated toward the leeward side of the body
$(\Delta\alpha)_{Vi}$	Average angle of attack induced on fin i by vortices
$\Delta\alpha_{eq}$	Increment in α_{eq}
η	Length factor in cross flow drag theory
λ	Fin taper ratio
Λ_{ji}	Fin deflection factor
ϕ_i	Roll angle of fin i